Journal of Power Sources 598 (2024) 234181

Contents lists available at ScienceDirect

Journal of Power Sources

journal homepage: www.elsevier.com/locate/jpowsour

Online estimation of the state of charge and state of health of a vanadium redox flow battery

Alejandro Clemente [a,b,*], Manuel Montiel [c,d], Félix Barreras [c], Antonio Lozano [c], Bryan Escachx [e], Ramon Costa-Castelló [b]

[a] *Institut de Recerca d'Energia de Catalunya (IREC), Jardins de les Dones de Negre 1, 08930 Sant Adrià del Besòs, Barcelona, Spain*
[b] *Universitat Politècnica de Catalunya, Avinguda Diagonal, 647, 08028 Barcelona, Spain*
[c] *Instituto de Carboquímica, CSIC, Miguel Luesma Castán, 4, 50018 Zaragoza, Spain*
[d] *Fundación Agencia Aragonesa para la Investigación y el Desarrollo (ARAID), Av. de Ranillas, 1-D, 50018, Zaragoza, Spain*
[e] *Institut de Robòtica i Informàtica Industrial, CSIC-UPC, Llorens i Artigues 4-6, 08028 Barcelona, Spain*

HIGHLIGHTS

- The model proposed considers mass and charge conservation principles.
- An online observer for both SOC and SOH indicators is developed.
- SOC and SOH estimations are obtained by only measuring the battery voltage.
- Numerical and experimental data has been used to validate the observer.
- Results show the possibility to properly estimate the SOC and SOH in real time.

GRAPHICAL ABSTRACT

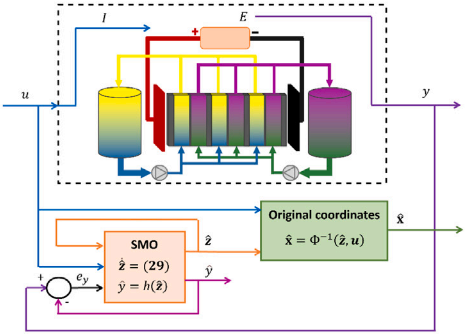

---

[*] Corresponding author at: Universitat Politècnica de Catalunya, Avinguda Diagonal, 647, 08028 Barcelona, Spain.
E-mail address: alejandro.clemente.leon@upc.edu (A. Clemente).

https://doi.org/10.1016/j.jpowsour.2024.234181
Received 8 November 2023; Received in revised form 15 January 2024; Accepted 1 February 2024

ARTICLE INFO

Keywords:
Nonlinear model
Redox flow battery
Sliding mode observer
Stack
State of charge
State of health
Particle swarm optimization

ABSTRACT

This study presents an online algorithm capable to simultaneously estimate the state of charge and state of health of a vanadium redox flow battery. Starting from a general electrochemical model, some order reductions are carried out considering different conservation laws. Based on these low-order models, the observer is designed considering the terminal voltage of the battery. This observer is firstly analyzed using numerical tools. Secondly, an experimental validation is carried out with real data provided by a vanadium redox flow battery stack, consisting on current and voltage measurements.

1. Introduction

Nowadays, the search of efficient, low-cost, safe and long-life energy storage systems (ESSs) is one of the topics of greatest interest. In the exploration of technologies that meet these criteria, vanadium redox flow batteries (VRFBs) have emerged as a prominent solution. Moreover, these devices have the particularity of decoupling energy and power, allowing for the definition of these variables in terms of electrolyte volumes and stack size, respectively.

On the one hand, the electrolyte volumes define the amount of energy the battery can store. Thus, they can be chosen according to the size of the tanks where they are contained. On the other hand, the power depends on the charging or discharging current and the battery voltage. Both variables depend on the stack size, in terms of electrode area and number of cells.

Regarding VRFBs, one of their significant advantages compared to other redox flow battery typologies is the minimal battery degradation resulting from the mixing of species on both sides, given that all electrolytes consist of vanadium species. Specifically, the anode comprises vanadium species V^{2+} and V^{3+}, leading to the valences V^{II} and V^{III}. On the other side, the cathode is composed of vanadium oxides VO^{2+} and VO_2^+, yielding the valences V^{IV} and V^{V}, respectively. Consequently, the concentration of each vanadium species is dependent on the redox reactions occurring within the cell that can be formulated as follows:

$$V^{2+} \rightleftarrows V^{3++e^-} \tag{1}$$

$$VO_2^+ + 2H^+ + e^- \rightleftarrows VO^{2+} + H_2O\,, \tag{2}$$

for the anode (1) and cathode (2) sides, where → denotes a discharging process and ← a charging one.

With respect to the voltage, typical values for a single cell composed by two electrodes and one membrane vary between 0.6 to 1.8 V considering a total discharged and charged battery, respectively. In order to increase the voltage of the VRFB system, a number of cells are assembled in electrical series to obtain what is commonly known as a stack. Fig. 1 shows the scheme of a VRFB made of 3 cells where it is possible to see the configuration required to assemble them conforming the stack.

Concerning the research inside the field of control and supervision of VRFBs, one of the most important challenges corresponds to the estimation of the state of charge (SOC) and state of health (SOH). Both battery indicators provide valuable information about the system performance and are typically required for the design of optimal control strategies, such as the control of the flow rates based on the Faraday's electrolysis law [1].

There is a large number of works in the literature focused on the SOC estimation of electrochemical devices [2]. Specifically, in a VRFB, the SOC is directly related to the amount of energy stored and its value depends on the proportion of vanadium species within each side. Therefore, there are different methods that have been developed to obtain a measurement of the species concentration such as the analysis of the electrolyte color or conductivity [3]. However, these techniques usually require an offline analysis and present an important lack of accuracy [4].

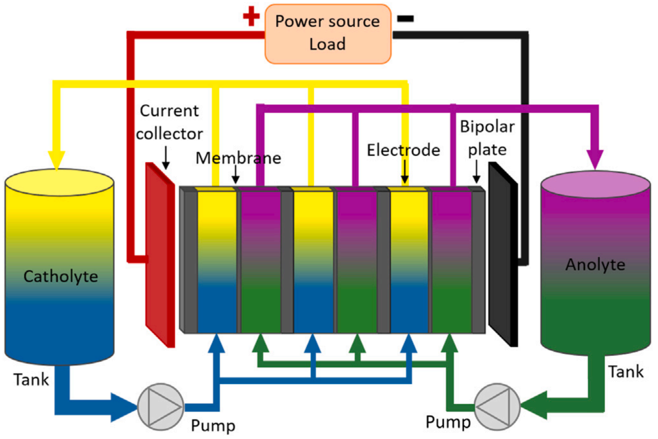

Fig. 1. Vanadium redox flow battery scheme composed of a stack with three cells.

Taking these drawbacks into account, a good alternative that is currently emerging is the use of state observers capable of estimating the SOC through other easily measurable variables such as the current or voltage [5]. Thus, it is possible to find a great number of studies dedicated to estimate the SOC of a VRFB using different typologies of observers. By means of the measurement of the open circuit voltage (OCV), the SOC has been successfully estimated in different works. Among the different observers used, the Extended Kalman Filter (EKF) or the Sliding Mode Observer (SMO) can be highlighted [6,7].

Nevertheless, vast majority of SOC observers use an equivalent electric circuit model (ECM) and the OCV measurement to obtain highly accurate estimations. This can be observed in works such as Xiong et al. [8] or Dong et al. [9], where they use ECMs to develop a SOC observer. In terms of precision, these works have proposed a valid observer capable of estimating the SOC accurately, with a root mean square error (RMSE) below 0.01 SOC [9].

In terms of SOH estimation there are few studies that present an observer capable to estimate its evolution for VRFBs. On the one hand, the SOH depends on many phenomena, such as mass imbalance due to ion crossover phenomenon, side reactions or improper operation [2]. Therefore, it is difficult to obtain a model that is capable of replicating the SOH evolution with high accuracy considering the aforementioned factors. Furthermore, the dynamics described by these phenomena are very slow compared to other processes such as the redox reactions that take place inside the stack almost instantaneously. For this reason, these slow phenomena are associated to a low observability in terms of online state estimation.

However, the SOH estimation problem has been presented and analyZed in other types of electrochemical systems such as lithium-ion batteries [10]. Typically, the estimation of both SOC and SOH is developed using ECMs where the SOH is normally associated to a capacitance. In Xiong et al. [8], a capacity fading factor was used. The results obtained in this study show accurate SOC estimation with a root mean square error (RMSE) below 0.013 V between the measured terminal voltage and the estimated one.

Other works have been validated with real experimental data such as a fast ECM-based estimation algorithm developed by Khaki et al. [11] or a EKF algorithm used to estimate the SOC and the capacity concurrently and presented in the work of Wei et al. [12]. Although these works have proposed partial solutions to the SOH estimation problem in VRFBs, they have certain limitations that should be highlighted. First of all, they are based on the use of ECMs where the SOH is described in terms of a capacitance which cannot be related to the vanadium species behavior. Furthermore, all these works consider the case of a single cell, without validating the case of a stack formed by multiple cells.

Recent works have proposed different techniques to estimate the SOH of a VRFB. This is the case of Vlaso et al. [13], which has presented a deterministic method based on the shift of electrolyte refractive index values at the same OCV. However, this work requires specific sensors that can increase the cost of the battery and can only be used under certain controlled operating conditions. Thus, the use of measurements such as the OCV or terminal voltage has not been exploited until now. In Puleston et al. [14], a SOC and SOH numerical observer is presented, considering an electrochemical model and the use of the OCV, presenting a relative error below 2%.

Thus, the aim of this work is to formulate an online SOC and SOH estimation algorithm that can deal with an electrochemical model. Specifically, the goal is to design an online estimator compatible with the VRFB model previously presented in our work [15]. This study introduces a comprehensive model for a VRFB, outlining key phenomena and variables, such as species concentration evolution, temperature, and pressure dynamics, among others. The electrochemical model described follows the formulation proposed by Skyllas-Kazacos and was validated using real experimental data. Some model parameters were calibrated through an offline estimator algorithm, the Particle Swarm Optimizer (PSO). Additionally, employing this offline PSO, the SOC and SOH estimation were validated, yielding promising results that demonstrate the feasibility of determining both indicators using voltage and current measurements.

Based on these promising results, the complete Skyllas-Kazacos model has been employed as a starting point to formulate the problem and present the equations defining the SOC and SOH indicators. Subsequently, the model has been simplified by considering various hypotheses and applying conservation principles such as mass and charge conservation laws. Using the reduced-order model, a SMO has been formulated and analyzed through various simulation tests. Finally, the study has been validated using real experimental data obtained from an experimental setup comprising a stack formed by 5 cells.

This work has been organized as follows. Section 2 presents the problem formulation introducing the original model, the reduced one using the different hypotheses and conservation laws, the voltage computation and the definition of the SOC and SOH indicators. Section 3 shows the design of the SMO and the observability analysis. Section 4 performs different numerical tests to validate the observer. Section 5 encompasses the experimental part, describing the experimental setup and the results obtained when the SMO is implemented. Finally, Section 6 presents the main conclusions.

2. Problem formulation

The dynamics of the vanadium species are presented based on the original electrochemical model of Skyllas-Kazacos. Based on these dynamics, it is possible to present the SOC and SOH equations as well as the voltage computation. Finally, with the application of the conservation principles, the model can be reduced to present the formulation of the problem.

2.1. Electrochemical model

The evolution of the four vanadium species concentrations inside a VRFB is presented in the work of Skyllas-Kazacos et al. [16]. This model determines the behavior of all vanadium species, considering the effects of current, flow rates, and the diffusion mechanism. It is important to note that, due to the difficulty in properly modeling certain undesired inefficiencies such as shunt currents or component degradation [17], these phenomena are usually neglected in SOC and SOH estimation problems. However, even without considering these electrochemical inefficiencies, this electrochemical model has been widely analyzed and validated [15].

Considering only the effect of the redox reactions and assuming that the electrolyte flow rates are high enough to ensure that the concentration inside the stack is equal to that on the tanks, it is possible to obtain the following 4th order model [16]:

$$\dot{\boldsymbol{x}} = \frac{I}{(N \cdot v^c + v^t) \cdot F} \cdot [1 \;\; -1 \;\; -1 \;\; 1]^{\mathrm{T}} \tag{3}$$

where $\boldsymbol{x} \in \mathbb{R}^4$ is the state vector $[x_2 \;\; x_3 \;\; x_4 \;\; x_5]^{\mathrm{T}}$ composed by the four vanadium species: $\mathrm{V^{II}}$ ($\mathrm{V^{2+}}$), $\mathrm{V^{III}}$ ($\mathrm{V^{3+}}$), $\mathrm{V^{IV}}$ ($\mathrm{VO^{2+}}$) and $\mathrm{V^{V}}$ ($\mathrm{VO_2^{+}}$). Therefore, each state corresponds to a vanadium species concentration expressed in units of $\mathrm{mol/m^3}$.

Regarding the model parameters, N is the number of cells that compose the stack, v^c is the cell volume, v^t is the tank volume and F is the Faraday's constant. With respect to the sign of the current I, it has been considered positive for a charging process and negative for a discharging one. From now on, to simplify the equations formulation, the term v^{elec} will be used to represent the volume of electrolyte on each side of the battery that can be computed as:

$$v^{elec} = N \cdot v^c + v^t \; . \tag{4}$$

It is important to remark that the presented model does not take into account side reactions such as vanadium ion crossover, hydrogen evolution rate (HER), or water crossover. These reactions have been studied and modeled in different works, as they have great importance in the system mass imbalance, which affects the battery SOH.

On one hand, concerning vanadium ion crossover, it is well known that there are three main phenomena: diffusion, migration, and convection, as discussed by Oldham et al. [18]. As mentioned, only the diffusion mechanism appears modeled in the work of Skyllas-Kazacos. However, specific works have been conducted to model the migration and convection mechanisms, such as those by Hao et al. [19] and Chou et al. [20], demonstrating their contribution to mass imbalance. As explained, these ion crossover reactions change the mass on each side of the system while maintaining the total system mass and charge equal. Thus, based on these conservation principles and to simplify the problem complexity, a single parameter will be used to determine the mass imbalance, encompassing all the ion crossover mechanisms mentioned, instead of defining all three phenomena.

On the other hand, concerning the HER or water evolution, there are also studies that have developed models for these ions. Oh et al. [21] have defined a 3D electrochemical model that considers the evolution of water ions on both sides of the VRFB. It has been observed that the water crossover mechanisms contribute to the overall electrolyte imbalance between the negative and positive sides of the VRFB system. Thus, as with vanadium ion crossover, this phenomenon contributes to the drop in SOH and can be modeled by means of the mass imbalance parameter. Finally, with respect to HER at the negative electrode of the VRFB, Sun et al. [22] present a quantitative method to determine the hydrogen evolution rate. It has been observed that the hydrogen ions have a direct effect on the computation of the Nernst equation according to the redox reactions that take place inside the cell. However, in the vast majority of studies, the influence of these hydrogen ions can be modeled by means of the standard electrode potential, E^{θ}, as shown in the works of Knher et al. [23], and is modeled in the voltage computation section of this work.

Finally, it is worth mentioning that all these described phenomena could be introduced to the model presented in Eq. (3). Concerning vanadium ion crossover, it would be necessary to add the equations describing the evolution of vanadium species, considering the diffusion, migration, and convection mechanisms. Regarding the accounting of HER and water ions, it would be necessary to expand the state vector, considering each of these new ions as states in the model.

2.2. Performance indicators

Using the previously described model, it is possible to compute different performance indicators such as the SOC, the SOH and the stack voltage.

2.2.1. SOC and SOH computation

There are different definitions to present the computation of both SOC and SOH. Usually, the SOC is directly computed in terms of vanadium species or by the relationship between the charge capacity and the nominal one. With respect to the SOH computation, it is commonly expressed in terms of the maximum capacity or in relation to the internal battery resistance.

In this work, the expressions presented in [15] have been used, enabling the computation of both indicators in terms of the vanadium species.

Therefore, the total SOC of the battery can be computed as the minimum SOC between the catholyte and anolyte sides:

$$\mathrm{SOC} = min\left(\mathrm{SOC}_{-}, \mathrm{SOC}_{+}\right) . \tag{5}$$

where SOC_{-} and SOC_{+} are the SOC in the anolyte and catholyte sides, respectively, which can be computed as follows:

$$\mathrm{SOC}_{-} = \frac{x_2}{x_2 + x_3} , \tag{6}$$

$$\mathrm{SOC}_{+} = \frac{x_5}{x_4 + x_5} , \tag{7}$$

The main advantage of using this definition is the possibility to distinguish between the SOC in each side. This is particularly relevant in the presence of mass imbalance, where the SOC of both sides may differ.

Furthermore, this notation allows to express the battery SOC in terms of the amount of substance, considering the electrolytes volumes:

$$\mathrm{SOC}_{-} = \frac{n_2}{n_2 + n_3} , \tag{8}$$

$$\mathrm{SOC}_{-} = \frac{n_5}{n_4 + n_5} , \tag{9}$$

where n denotes the number of moles of vanadium species and can be computed for any particular species V^i considering the electrolyte volume:

$$n_i = v^{elec} \cdot x_i . \tag{10}$$

With respect to the SOH, using the same notation in terms of amount of vanadium n, it is possible to express its dynamics as:

$$\mathrm{SOH} = \frac{min\left(n_{-}, n_{+}\right)}{n^{*}} , \tag{11}$$

being n_{-} and n_{+} the moles of vanadium in the negative and positive sides, that can be computed as:

$$n_{-} = v^{elec} \cdot x_2 + v^{elec} \cdot x_3 , \tag{12}$$

$$n_{+} = v^{elec} \cdot x_4 + v^{elec} \cdot x_5 . \tag{13}$$

The term n^{*} is the initial number of vanadium moles of each one of the sides, which under ideal conditions of an initial balanced VRFB is equal for both sides. Therefore, it is possible to calculate its value as the half part of the total amount of substance n of the system:

$$n^{*} = \frac{n}{2} , \tag{14}$$

where n can be computed as the sum of the number of moles in the positive and negative sides:

$$n = n_{-} + n_{+} . \tag{15}$$

2.2.2. Voltage computation

The voltage of a VRFB depends on the species concentration, in the same way as both SOC and SOH. The VRFB voltage can be computed as the sum of the OCV and different overpotentials such as the ohmic, the activation and the concentration ones.

Regarding activation and concentration overpotentials, their impact can be mitigated by operating the battery at low current densities and within conditions where the SOC is constrained between 20% and 80% [24]. Additionally, treatments such as employing high-performance electrodes with oxygen-enriched thermal activation have been explored to decrease their contribution [25], resulting in a possible reduction of activation overpotential by 100 to 140 mV at operationally relevant current densities. For VRFBs, various studies like Delgado et al. [26] and Noren et al. [27] provide expressions for these overpotentials. They are based on the use of the Butler–Volmer equation, which defines the overpotentials in terms of current densities and species concentrations. With respect to the activation overpotential, which can be significant even at low currents, it can be simplified by linearizing the Butler–Volmer equation. In this context, the contribution of activation losses can be represented by a simple resistor. Considering these insights and with the goal of simplifying the formulation of the terminal voltage, it is assumed that, in comparison to ohmic losses, activation and concentration overpotentials have a negligible contribution, which, in any case, can be represented by an unknown resistor.

With respect to the ohmic losses, they are typically associated with an ohmic resistance related to the resistivity of the materials composing the different parts of the stack. Although this resistance may vary for each individual cell based on factors such as assembly position or thickness, it is commonly assumed to be equal for all cells within a stack [2]. Therefore, ohmic losses can be computed by considering the sum of resistances of all cells that make up a stack or by directly defining a total battery resistance term.

Taking these aspects into account, it is possible to formulate the voltage expression used in this work by means of the following equation [23]:

$$E = N \cdot \left(E^{\theta^{*}} + \frac{R \cdot T}{F} ln\left(\frac{x_2 \cdot x_5}{x_3 \cdot x_4}\right) + r \cdot I \right) \tag{16}$$

being $E^{\theta^{*}}$ the standard reduction potential that takes into account the concentration of protons, R the ideal gas constant, T the cell/stack temperature and r the ohmic resistance of an individual cell.

Both parameters $E^{\theta^{*}}$ and r have not theoretical values and are usually estimated offline [6]. Moreover, with respect to the resistance r, it has been found that its value can be different for a charging or discharging process. Therefore, it is necessary to differentiate between charging resistance r_c and discharging resistance r_d:

$$r = \begin{cases} r_d & I < 0 \\ r_c & I > 0 . \end{cases} \tag{17}$$

It is important to note that this voltage model assumes that all cells are equal in terms of voltage computation, given the well-established fact that cells within the stacks typically exhibit similar voltages. However, it is intriguing to analyze the potential occurrence of a cell problem within the stack.

If a cell exhibits damage, various phenomena may occur, including the generation of undesired gases such as hydrogen that can lead to the rapid degradation of the cell and the electrolytes. Under this issue, one cell can experience a high voltage. However, when dealing with stacks of multiple cells, a high cell voltage can potentially be compensated by the voltages of the other cells. Therefore, the model should continue to function properly within reasonable limits.

A defective operation can also manifest as a lower voltage for a specific current, resulting in a lower total stack voltage. When more current is demanded, there comes a point where the voltage of that specific cell reaches zero, and then it reverses. At this stage, the current no longer increases, and the potential reversal can spread to adjacent cells [28].

In this work, as only the terminal voltage of the stack is considered, it is not possible to identify which specific cell may have a problem. Therefore, this situation is beyond the scope of this study. In the event of significant damage to one or more cells, the proposed model, which relates the input current to the output voltage, should be modified to obtain an accurate estimation. Otherwise, the developed model will introduce a significant error that will be reflected in unexpected results concerning the SOC and SOH estimation when the observer is employed.

2.3. VRFB conservation principles

Considering the battery as an isolated system without any leaks, it is possible to satisfy certain conservation principles such as the laws of matter and charge conservation.

On one hand, the matter conservation principle can be proven analyzing the dynamics of the total number of moles n computed by Eq. (15). Substituting the dynamics expressed by Eq. (3) in Eq. (15) it is possible to see that the amount of matter is invariant. Thus, the total number of vanadium moles in the battery remains constant along the time.

On the other hand, the charge conservation principle can also be proven. The charge of a VRFB, denoted as ς, is directly related with the valence of the different vanadium species, being 1 for the vanadium species VO_2^+, 2 for the species V^{2+} and VO^{2+} and 3 for the vanadium species V^{3+}. Thus, the total charge can be computed as the sum of all vanadium species moles multiplied by their respective valences. Taking into account this definition, the charge conservation principle can be analyzed introducing in (15) the valences of the vanadium species and considering the same Eq. (3) to compute their dynamics. Similarly to the matter conservation analysis, the total charge is invariant remaining constant along the time under the mentioned conditions.

2.4. Reduced order model

Assuming that the total number of moles is initially known, it is possible to compute the total matter and charge, respectively. Therefore, as these values are constant, it is possible to simplify the original 4th order-model to a 2nd order-model.

Moreover, introducing the concept of mass imbalance, which can be defined as the difference of mass of the positive or negative side with respect to its original one, it is possible to reduce one more state assuming that this imbalance is known. Thus, it is possible to reduce the order-model in terms of n_+ (or n_-) according to Eq. (13). With the inclusion of this term, it is possible to consider the impact of crossover in the battery model, such as the vanadium ion crossover due to diffusion, migration, and convection mechanisms, or the influence of the hydrogen evolution reaction (HER) and water ions on the system imbalance. Although due to these phenomena it is known that n_+ is not constant, its variation is very slow compared to the species concentration dynamics, so it can be considered as a parameter. As can be noticed from (13), n_+ is linearly independent of (15). Considering this property, it is possible to derive a 1st order-model with two known parameters, n and ς, and one unknown parameter, n_+.

Thus, using as state the vanadium species V^{2+}, its dynamics is given by the following expression:

$$\dot{x}_2 = \frac{I}{\upsilon^{elec} \cdot F} \;, \tag{18}$$

and the concentrations of the other vanadium species can be computed as:

$$x_3 = -\frac{x_2 \cdot \upsilon^{elec} - n + n_+}{\upsilon^{elec}} \tag{19}$$

$$x_4 = -\frac{x_2 \cdot \upsilon^{elec} - 3n - \varsigma - 2n_+}{\upsilon^{elec}} \tag{20}$$

$$x_5 = \frac{x_2 \cdot \upsilon^{elec} - 3n + \varsigma - n_+}{\upsilon^{elec}} \;. \tag{21}$$

Finally, by substituting expressions (19)–(21) in (16), it is possible to formulate an estimation problem by computing the evolution of x_2 using the voltage measurement E, obtaining the following system:

$$\begin{aligned} \dot{x}_2 &= \frac{I}{\upsilon^{elec} \cdot F} \\ E &= h(\boldsymbol{x_2}, n, \varsigma, n_+) \;, \end{aligned} \tag{22}$$

where h is the voltage nonlinear function defined by Eq. (16).

It is important to note that if the exact amount of substance n_+ is known, the SOH can be directly computed and the problem will only consists on the estimation of the SOC by estimating x_2. However, in the case where n_+ is unknown, solving the formulated problem requires the joint estimation of x_2 and n_+ to compute the battery SOC and SOH. Regarding this situation, it is important to describe two possible cases of study. During short-time period scenarios, the crossover does not have a significant impact on the model performance, and it is only necessary to estimate the value of n_+ considering it as a parameter. However, in long-time period scenarios, the evolution of the crossover impact becomes apparent. Therefore, under these circumstances, it is necessary to consider the term n_+ as a variable to be estimated.

3. Observer design

The sliding mode controller (SMC) is one of the most common techniques used in nonlinear systems for both control and observer applications [29]. Its working principle involves creating a sliding surface where convergence is intended, along with a feedback term designed to bring the system within this surface. If this control action is well-designed, the system dynamics are stable and will converge to the sliding surface in finite time. Thus, for the particular case of estimation problems, the estimated values will be very similar to the real ones [30]. The use of sliding mode observers (SMOs) for State of Charge (SOC) monitoring is prevalent in the literature, with works such as Du et al. [31] and Xiong et al. [32], designing an SMO to estimate the SOC of a lithium-ion and redox flow battery, respectively.

To properly design the observer, the following procedure has been developed. Firstly, a SMO has been formulated considering a general non-linear system that can be directly related to the VRFB model presented in Section 2. Secondly, an observability analysis has been computed to guarantee that the states of the non-linear system can be estimated using the formulated observer.

3.1. Sliding mode observer formulation

There are many different ways to define an SMO. In this work, it has been decided to implement the method explained in Cecilia et al. [33], which can be used for observers with input uncertainty.

Considering a non-linear system expressed as:

$$\begin{aligned} \dot{\mathbf{x}} &= \boldsymbol{f}(\mathbf{x}, \boldsymbol{u}) \\ y &= h(\mathbf{x}) \;. \end{aligned} \tag{23}$$

where $\mathbf{x} \in \mathbb{R}^n$ is the state vector, $\boldsymbol{u} \in \mathbb{R}^m$ is the input vector and $\boldsymbol{f}$ is the vector field. From this formulation, if the system output y has relative degree n, it is possible to express the same system dynamics in controllable canonical form (CCF) by means of the following change of variables [34]:

$$\boldsymbol{z} = \boldsymbol{\phi}(\mathbf{x}) = \begin{bmatrix} y \\ \dot{y} \\ \vdots \\ y^{(n-1)} \end{bmatrix} = \begin{bmatrix} h(\mathbf{x}) \\ L_f h(\mathbf{x}) \\ \vdots \\ L_f^{n-1} h(\mathbf{x}) \end{bmatrix} \tag{24}$$

where $L_f h(\mathbf{x})$ is the Lie derivative and can be computed as follows:

$$\begin{aligned} L_f h(\mathbf{x}) &= \frac{\partial h(\mathbf{x})}{\partial \mathbf{x}} \cdot \boldsymbol{f}(\mathbf{x}, \boldsymbol{u}) \\ L_f^n h(\mathbf{x}) &= \frac{\partial L_f^{n-1} h(\mathbf{x})}{\partial \mathbf{x}} \cdot \boldsymbol{f}(\mathbf{x}, \boldsymbol{u}) \,. \end{aligned} \tag{25}$$

As long as the $\boldsymbol{\phi}(\mathbf{x})$ transformation is a diffeomorphism, trajectories in the new coordinate system $\boldsymbol{z}$ will have unique counterparts in the original $\mathbf{x}$ coordinate system that are also smooth.

Thus, it is possible to compute the dynamics of the new coordinates z as:

$$\dot{\boldsymbol{z}} = \begin{bmatrix} \dot{z}_0 \\ \dot{z}_1 \\ \vdots \\ \dot{z}_{n-1} \\ \dot{z}_n \end{bmatrix} = \begin{bmatrix} z_1 \\ z_2 \\ \vdots \\ L_f^{n-1} h(\mathbf{x}) \\ L_f^n h(\mathbf{x}) \end{bmatrix} \tag{26}$$

which represent a triangular form. For this particular structure, it is possible to design a higher-order sliding mode observer that takes the following form [29,33]:

$$\dot{\hat{\boldsymbol{z}}} = \begin{bmatrix} \hat{z}_1 - \lambda_0 |\hat{z}_0 - y|^{(n/n+1)} sign(\hat{z}_0 - y) \\ \hat{z}_2 - \lambda_1 |\hat{z}_1 - \dot{\hat{z}}_0|^{(n-1/n)} sign(\hat{z}_1 - \dot{\hat{z}}_0) \\ \vdots \\ \hat{z}_n - \lambda_{n-1} |\hat{z}_{n-1} - \dot{\hat{z}}_{n-2}|^{(1/2)} sign(\hat{z}_{n-1} - \dot{\hat{z}}_{n-2}) \\ -\lambda_n sign(\hat{z}_n - \dot{\hat{z}}_{n-1}) \end{bmatrix} \tag{27}$$

where $\dot{\hat{\boldsymbol{z}}}$ is used to denote the estimation of the state dynamics $\dot{\boldsymbol{z}}$, n stands for the order of the model, λ_i are the observer parameters to be tuned and $sign(\cdot)$ is the sign function that can be computed as:

$$sign(a) = \begin{cases} \dfrac{a}{|a|} & \text{if } a \neq 0 \\ 0 & \text{if } a = 0 \end{cases} \tag{28}$$

Thus, it is possible to formulate (27) in terms of the output error, which can be computed as $e_y \triangleq \hat{y} - y$[1]:

$$\dot{\hat{\boldsymbol{z}}} = \begin{bmatrix} \hat{z}_1 - \lambda_0 |e_y|^{(n/n+1)} sign(e_y) \\ \hat{z}_2 - \lambda_1 |\dot{e}_y|^{(n-1/n)} sign(\dot{e}_y) \\ \vdots \\ \hat{z}_n - \lambda_{n-1} |\overset{\dot{n-1}}{\mathrm{e}}_y|^{(1/2)} sign(\overset{\dot{n-1}}{\mathrm{e}}_y) \\ -\lambda_n sign(\overset{\dot{n}}{\mathrm{e}}_y) \end{bmatrix} \tag{29}$$

One of the greatest advantages of this type of high-order estimators is that the computation of the state dynamics follows a recursive procedure from the last equation to the initial one. This can be seen looking (27) where it is possible to observe that the last term to compute $\dot{\hat{z}}_i$ corresponds to the previous state $\dot{\hat{z}}_{i-1}$. This recursive procedure occurs from the last state $\dot{\hat{z}}_n$ until the initial one $\dot{\hat{z}}_0$ where the last term corresponds to the output measurement y.

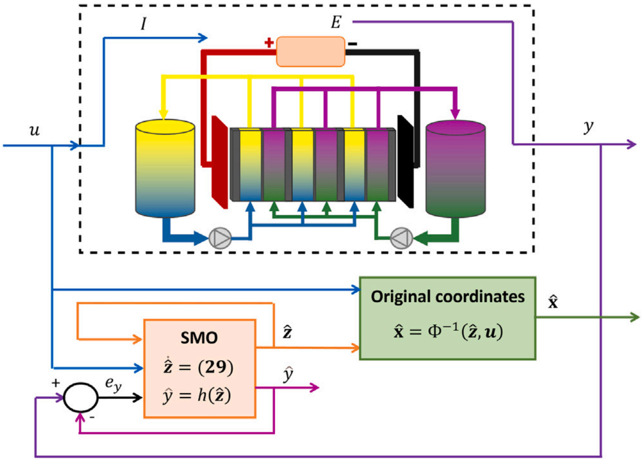

Fig. 2. Observer scheme for the VRFB.

Thus, it is important to remark that using this state estimator it is only necessary to compute the output error e_y, differing from the classical SMO that requires to compute all error derivatives that appear in (29) using the derivatives of the output function, which can lead to several problems such as noise and uncertainty phenomena. This can be observed in Fig. 2, which illustrates a schematic representation of the proposed SMO for the VRFB. As depicted, for the state estimation, it is only necessary to compute the output signal y, corresponding to the terminal voltage E.

It is important to note that the set of parameters λ_0, $\lambda_1 \ldots$ λ_n are positive and must be tuned in order to ensure that the observer estimation converges to zero. There are different ways to compute the values of λ to ensure the correct convergence of the state estimator. Works such as [33,35] present a methodology to tune the aforementioned parameters considering the case of high-order sliding mode observers (HOSM). This methodology is based on the use of a family of Lyapunov functions (LF) that makes possible to estimate the convergence time or the robustness against measurement noise.

Following the general methodology presented in [35], the observer design parameters λ can be defined as:

$$\lambda = \begin{bmatrix} \lambda_0 \\ \lambda_1 \\ \vdots \\ \lambda_{n-1} \\ \lambda_n \end{bmatrix} = \begin{bmatrix} \kappa_0 M^{(1/n)} \\ \kappa_1 M^{(2/n)} \\ \vdots \\ \kappa_{n-1} M^{(n-1/n)} \\ \kappa_n M \end{bmatrix} \tag{30}$$

being M the upper bound of the last system derivative $\dot{z}_n$ such that $|\dot{z}_n| \leq M$.

The set of parameters κ are positive parameters that are usually chosen by computer simulation or can be found using a recursive procedure [35]. The estimation error will converge to zero if κ_i are positive constants such that the polynomial

$$s^n + \kappa_0 s^{n-1} + \kappa_1 s^{n-2} + \cdots + \kappa_{n-1} s + \kappa_n \tag{31}$$

is Hurwitz, which means that has all the roots in the left half-plane [36].

If these two conditions are met, the observer will converge to the real value with null error in finite time. regarding the selection of the parameter κ_i, it directly influences the convergence time and sensitivity to disturbances. Considering the case of a 1st order-model with a unique parameter κ_0, higher values of κ_0 enable a faster estimation, but makes the estimation more sensitive to disturbances such as measurement noise. Conversely, lower values of κ_0 exhibit the opposite behavior.

Therefore, there must be a trade-off between both convergence time and sensitivity. When dealing with noisy systems, the establishment

---

[1] To formulate the derivatives of the output error e_y, the following notation is used $\overset{i}{\mathrm{e}}_y$ where the subscript i represents the ith derivative.

time may need to be sacrificed by using small observer gains κ_i to ensure a correct estimate with low noise. On counterpart, when dealing with non-noisy systems, faster convergence can be achieved by using high values of κ_i.

Although it is not straightforward to define a tuning methodology because it depends on the concrete experimental setup (i.e. it depends on the measurement noise), there are some theoretical works focused on this topic which offer concrete tuning methodologies [37].

3.2. Observability analysis

Before the implementation of the observer it is important to introduce the concept of observability. The observability of a system is the property that determines if the internal states can be inferred through the external outputs. Thus, for the VRFB, the system defined in (22) will be called observable if the state x_2 can be inferred from the output y.

For any non-linear system as the ones proposed in this work, it is possible to determine its observability through the analysis of the observability codistribution, Ω_s, rank [38]. If the rank is equal to the number of states, the system is called observable. Otherwise, not all states can be reconstructed from the output system. The computation of Ω_s can be formulated as:

$$\begin{aligned}\Omega_s &= span\{\nabla h(\mathbf{x})\} \oplus span\{\nabla L_{\dot{\mathbf{x}}} h(\mathbf{x})\}\\ &\oplus span\{\nabla L^2_{\dot{\mathbf{x}}} h(\mathbf{x})\} \ldots \oplus span\{\nabla L^{n-1}_{\dot{\mathbf{x}}} h(\mathbf{x})\}\end{aligned} \tag{32}$$

where $\oplus$ is the direct sum operator, h is the output function, and L^i is the ith Lie derivative function. As can be noticed, the computation of Ω_s requires the same functions used in the formulation of the SMO, being possible to relate Ω_s to the jacobian of $\boldsymbol{\phi}$.

4. Numerical validation

To analyze the behavior of the SOC and SOH estimator, various cases have been numerically analyzed. In order to perform this numerical analysis, it has been chosen a VRFB composed by a single cell, two reservoirs of 100 ml and a total vanadium concentration of 1600 mol/m^3.

Considering the amount of electrolyte that is imposed by the reservoirs capacity and the electrolytes concentration, it is possible to compute the total number of moles and charge, n and ς, resulting:

$$\begin{aligned} n &= 0.32\ ,\\ \varsigma &= 1.12\ . \end{aligned} \tag{33}$$

Before implementing the observer, it is important to study the dependence of the system dynamics with respect to n and ς parameters. This analysis will provide information about how sensitive is the simplified model.

To perform this initial study, the evolution of x_5 has been analyzed. As can be noticed from Eq. (21), its value depends on x_2 and some model parameters. On one hand, the evolution of x_2 only relies on the current and electrolyte volumes according to (18). On the other hand, the total number of moles n has been changed while the total charge ς remains constant. Moreover, it has been considered that the system is balanced being n_+ exactly half of n.

Under these conditions, if there is a difference between the considered n with respect to the real value in (33), it will exist a difference between x_2 and x_5. Fig. 3 shows the behavior of x_5 when different values of n are considered assuming a constant ς, and a charging and discharging process at constant current of 2 A.

As can be noticed from Fig. 3, when n takes the real value, the evolution of x_5 (in blue) is equal to x_2. However, if n is changed increasing its value, the evolution of x_5 also changes, existing an important error.

For the case of presenting a 0.3125% relative error with respect to the real value (case of $n = 0.321$), there exists a constant gap of 35 mol/m^3, which can be seen as a relative error of at least 4.2% along the cycle. The gap grows considerably for a relative error of 3.125% (case of $n = 0.330$). In this case, the gap between the real value of x_2 and the estimated one is approximately 350 mol/m^3, which corresponds to an error higher than 40% along the charging and discharging process.

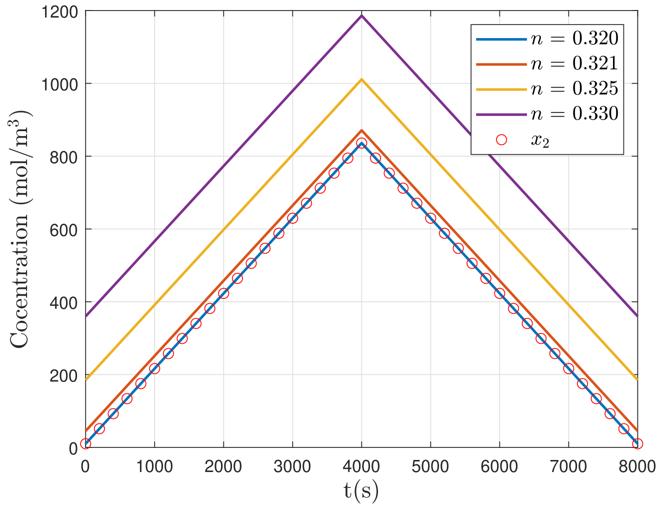

Fig. 3. x_5 evolution during a charging and discharging process at 2 A for different values of n considering that $\varsigma = 1.12$ and the system is balanced. (For interpretation of the references to color in this figure legend, the reader is referred to the web version of this article.)

Therefore, for the development of the SOC and SOH estimator using the reduced model presented in (22), it is necessary to accurately compute the system's amount of matter, n, and charge, ς, or employ an observer capable of operating under situations of parameter uncertainty.

4.1. State of charge estimation

The first analysis that has been carried out is the estimation of x_2 assuming that n_+ is known and constant. Thus, the model consists on the first order-model system formulated by Eq. (22).

For this particular case, the observability analysis is straightforward. As there is only one state to be estimated, the SOC can be directly observed by means of the output signal y. Therefore, it is possible to implement the observer structure defined in Eq. (27) corresponding to a 1st order-model. Thus, the observer takes the following form:

$$\dot{\hat{z}}_0 = -\kappa_0 M \cdot sign(e_y) \tag{34}$$

being $e_y = \hat{z}_0 - y$ the error between the estimated voltage and the real one E computed by means of expression (22).

As can be observed from Eq. (34), the parameters to select are κ_0 and M. According to the estimator theory described in the previous section, for this 1st order-model, the parameter M must be greater than the output derivative, $\dot{y}$, which corresponds to the voltage derivative.

In order to find the value of M, an analytic analysis has been developed consisting on determining the bounds of the voltage derivative. Considering the voltage function which depends on the state x_2 and the input current I according to expression (22), it is possible to compute the output derivative $\dot{y}$ as:

$$\dot{y} = \frac{\partial h}{\partial x_2} \cdot \dot{x}_2 + \frac{\partial h}{\partial I} \cdot \dot{I}\ . \tag{35}$$

From this equation, it is possible to obtain analytically the bounds of $\dot{y}$. In the Appendix section it is shown the process developed to obtain the analytical expression of $\dot{y}$ and its possible derivatives, which can be required for higher-order models.

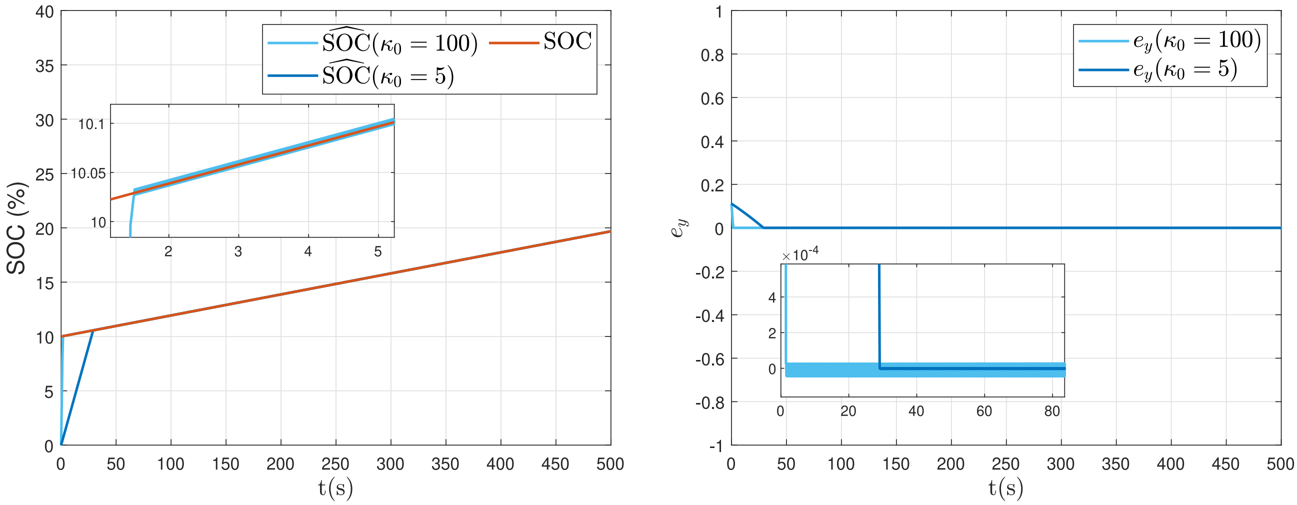

(a) Ideal conditions.

(b) Output error.

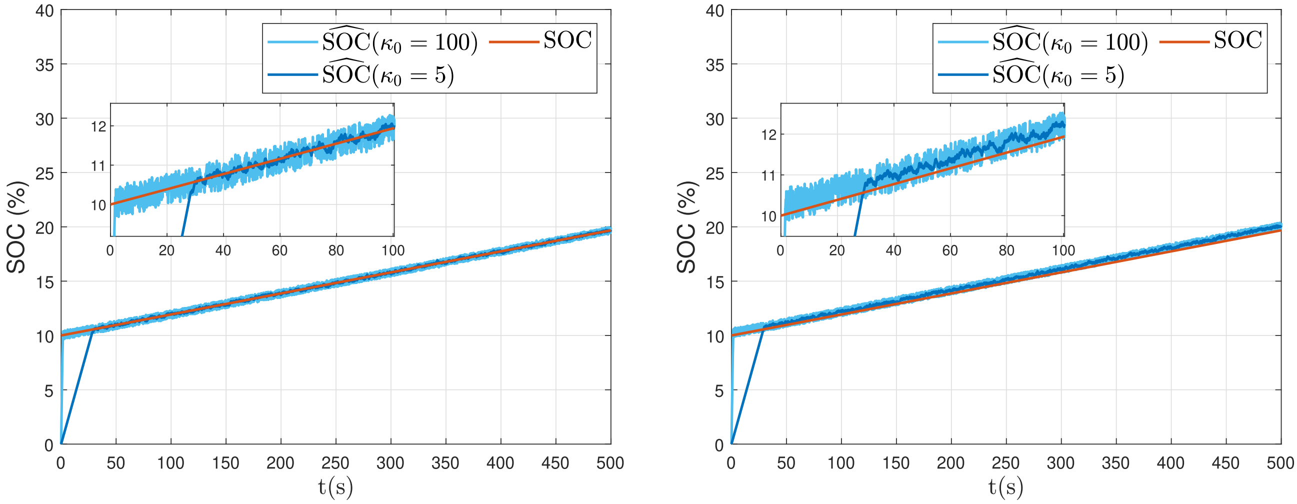

(c) Measurement noise.

(d) Parameter uncertainty.

Fig. 4. SOC estimation for a charging process at constant current of 2 A considering different values of κ_0. (a) Real (red) and estimated SOC evolution (blue) under ideal conditions. (b) Output error e_y evolution under ideal conditions. (c) Real (red) and estimated SOC dynamics (blue) in the presence of measurement noise in the output function. (d) Real (red) and estimated SOC dynamics (blue) in the presence of measurement noise and parameter uncertainty. (For interpretation of the references to color in this figure legend, the reader is referred to the web version of this article.)

Thus, to compute numerically the lower and upper bounds of $\dot{y}$ it is only necessary to define the bounds of both I and x_2 variables.

With respect to the current, for a single VRFB as the one presented in this numerical analysis, typical values of current varies between 1 and 3 A [39]. Therefore, in order to make a realistic and reliable numerical study it has been considered a higher bound of 4 A.

With respect to the concentration x_2, theoretically it can only vary between 0 and the total vanadium concentration which in this case is 1600 mol/m^3. However, it is important to remark that in practical applications, it is not recommended to take the battery to extreme levels of charge or discharge, due to the appearance of secondary reactions. Normally the SOC operating range varies between 10 to 90% to avoid these undesired phenomena [40].

Thus, for this case of study, it has been considered a bound between 150 mol/m^3 to 1440 mol/m^3. Taking into account these values, it has been found that M must be positive and greater than $2 \cdot 10^{-3}$ to accomplish the condition of upper bound.

Once the value of M has been selected ($1 \cdot 10^{-1}$ for this particular example) it is only necessary to choose the value of the parameter κ_0. As has been explained, it must be positive ensuring that the polynomial defined by Eq. (31) has the root in the left half-plane. Different values of gain κ_0 have been considered to analyze the observer performance.

Fig. 4(a) shows the SOC profile when a charging process at constant current of 2 A takes place. In order to validate the results, the estimated SOC ($\widehat{\mathrm{SOC}}$) has been compared with the original one obtained with the 4th order-model under the same mentioned conditions.

As can be noticed, the gain κ_0 has a direct effect in the estimation response time. Lower values of κ_0 increase the convergence time. It is also possible to analyze the error dynamics, which in this case corresponds to the difference between the real voltage and the estimated one. The behavior obtained is similar to the ones observed for the SOC dynamics.

First of all, as can be noticed in Fig. 4(b), it is important to remark how the error converges to zero in finite time. For the case of $\kappa_0 = 100$, the steady-state behavior of the error is found in less than 2 s, but presenting a gap that varies between −4 and $2 \cdot 10^{-5}$. Considering the other case with $\kappa_0 = 5$, the error converges to zero in almost 30 s and the gap of the sliding surface is almost null as can be observed in the detail.

Taking into account these results it seems appropriate to choose high values of κ_0 in order to obtain a faster estimation. However, it must be noted that the sliding surface also increases as can be noticed in the details of Fig. 4(a) and (b) for the SOC and error dynamics, respectively.

At this point, it is important to analyze the behavior of the presented observer under undesired phenomena such as parameter uncertainty or measurement noise in the output or input signals. Taking into account all these possible situations, the value of M must be recomputed, which can be developed numerically introducing the limits of these phenomena and performing a simulation to find the upper values of the output function and its derivatives.

With respect to κ_0, under the presence of measurement noise, the effect of high values of κ_0 is negative getting a noisier estimation. Fig. 4(c) shows the SOC estimation when the output presents noise with a Gaussian distribution with 0.002 variance. As can be noticed, under this situation, the estimation is noisier with high values of κ_0 while the noise is practically null taking lower values.

Finally, it is important to analyze the case of uncertainty in the system parameters such as the total number of moles n or the charge ς. In order to develop this analysis, it has been considered the previous profile, introducing a 10% of variation of n.

As has been previously discussed, the system sensitivity on the parameter uncertainty can be handled by means of the SMO gain κ_0. Fig. 4(d) shows the SOC estimation where it is possible to see how under the conditions of uncertainty mentioned, there exist a constant error between the SOC obtained from the original model and the estimated one $\widehat{SOC}$. This constant error appears due to the fact that the parameter n appears in the diffeomorphism. Therefore, it is important to obtain good measurements of both ς and n in real applications.

As a general observation across all studied cases, it can be concluded that the estimation error decreases with low values of the κ_0 parameter, but the convergence time is higher. Hence, it is necessary to find a compromise between various characteristics, including the convergence time, sensitivity to output measurement noise, and parameter uncertainty.

Taking into account the results obtained from the different analyses, where the original 4th order-model was compared to the simplified one by means of an observer, it is possible to conclude that the SOC estimator presents good results being possible to modify its robustness in terms of the κ_0 parameter.

4.2. State of charge and state of health estimation

Considering n_+ as a unknown parameter that must be estimated, the problem focuses into the estimation of both SOC and SOH indicators. As has been explained, the amount of vanadium in the positive side n_+ is associated to the SOH, varying its value when the imbalance phenomena take place. Usually, the lost of capacity due to this electrolyte imbalance is so slow that can be considered as constant in short-medium intervals of time [41]. However, reasonable studies have defined a slow and linear SOH tendency along the cycles [7].

Thus, this work presents a SOC and SOH estimator for two cases. The first one consists in the estimation of the SOC and SOH assuming that n_+ is a constant unknown parameter. In the second one, the SOH is not assumed constant and to contemplate this behavior a model with state perturbation has been defined.

Taking into account these two cases, it is possible to formulate a 2nd and a 3rd order-model systems using the same output function h, which corresponds to the VRFB voltage denoted as E. For both cases, the observability analysis has been developed and the observer is computed following the theory explained in the previous section.

For the first case of study it is possible to formulate the new system dynamics as:

$$\dot{\boldsymbol{x}} = \begin{bmatrix} \dfrac{I}{\upsilon^{elec} \cdot F} \\ 0 \end{bmatrix} \qquad (36)$$

$$y = h(\boldsymbol{x_2}, n, \varsigma, n_+)$$

being $\boldsymbol{x} = [x_2 \;\; n_+]^\top$ the new state vector that considers the previous state x_2 and the amount of vanadium in the positive side n_+. Thus, the problem becomes a second order-model with two unknown states that appear directly in the output function y.

As can be noticed, with the dynamics formulated by means of (36), n_+ is considered as a parameter. Using this formulation it is possible to use the second-order SMO to estimate the value of both x_2 and n_+ states, that is translated in the SOC and SOH estimation.

Before implementing the aforementioned observer, an observability analysis has been developed in order to see if both states can be estimated using the system output y. By means of the computation of Ω_s as was described in (32), it has been found that the rank of Ω_s is 2, being the number of states of $\boldsymbol{x}$. Therefore, the system dynamics presented in Eq. (36) are observable.

Once the observability analysis has been performed, it is possible to define the SMO for the 2nd order-model system which takes the following form:

$$\begin{aligned} \dot{\hat{z}}_0 &= \hat{z}_1 - \kappa_0 M^{1/2} |\hat{z}_0 - y|^{(1/2)} \cdot \, sign(\hat{z}_0 - y) \\ \dot{\hat{z}}_1 &= -\kappa_1 M \cdot sign(\hat{z}_1 - \dot{\hat{z}}_0) \, . \end{aligned} \qquad (37)$$

As can be noticed, for this second-order observer, in the second equation appears in the last term the variable $\dot{\hat{z}}_0$ which can be directly computed by means of the previous equation and the system output y. Therefore, for this particular case there are two κ parameters to be tuned and the same parameter M previously bounded.

Taking into account this model, the parameter M must be found as the upper bound of the second voltage derivative $\ddot{y}$, following the theoretical procedure presented in [35]. Thus, its value can be computed performing the derivative of the function $\dot{y}$, which appears in the Appendix, following the previous procedure shown. For this particular case, as the second voltage derivative equation $\ddot{y}$ is long to be computed it has been omitted.

As has been done with the previous case of study, it has been performed an analysis to estimate both SOC and SOH when a charging process takes place from an initial discharged balanced system.

In order to analyze the estimation of both SOC and SOH using the second-order system, the same scenario previously defined has been used.

As can be observed in Fig. 5, both SOC and SOH are estimated with great accuracy.

Looking Fig. 5(a), it can be noted that the time required to estimate the SOC is less than 10 s, appearing the sliding surface along the SOC dynamic. With respect to the SOH, the estimation requires a similar convergence time, as can be seen in Fig. 5(b). From these obtained results it is possible to validate the SOC and SOH observer in short time periods.

In order to validate the estimation at long time periods, a new simulation has been carried out where the SOH from the original 4th order-model decreases linearly along the time from an starting 97%. The selected total time is $t_{\text{tot}} = 50\,000$ s, while the SOC range is 0%–25% SOC in 1500 s.

Using the same second-order observer presented in Eq. (37) the results obtained are the ones shown in Fig. 6. As can be seen in Fig. 6(a), the SOC estimation stills converge with null steady-state error. However, with respect to the SOH, when it evolves along the time, its estimation using the previous observer carries an error and oscillations as can be seen in Fig. 6(b). This result is expected, as the observer has been designed with the purpose of estimating the SOH when is assumed constant. Therefore, if it is intended to estimate the SOH when its value decreases along the time according to the evolution seen in Fig. 6(b), a new observer must be designed.

The solution that is proposed in this work is to develop a model with state perturbation to be able to model the SOH dynamic. Thus, considering n_+ as a state to be estimated it is possible to formulate the

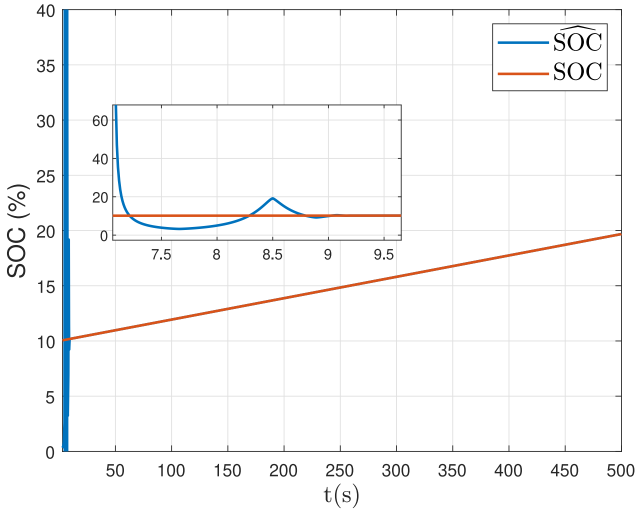

(a) SOC.

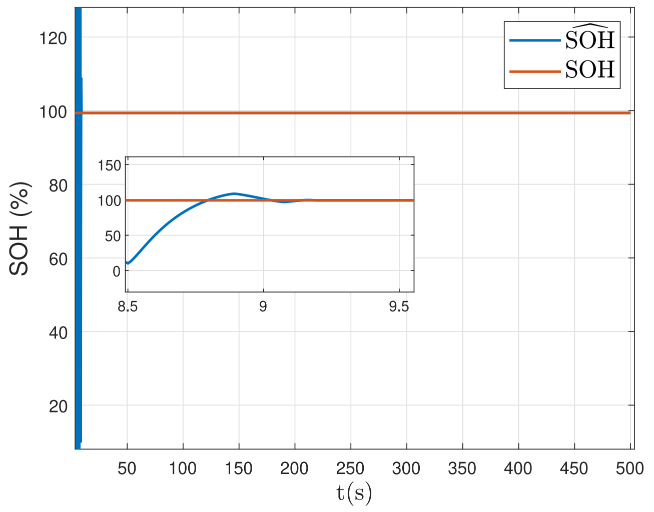

(b) SOH.

Fig. 5. Real (red) and estimated (blue) SOC and SOH dynamics when n_+ is constant and is assumed constant in the reduced 2nd order-model. (For interpretation of the references to color in this figure legend, the reader is referred to the web version of this article.)

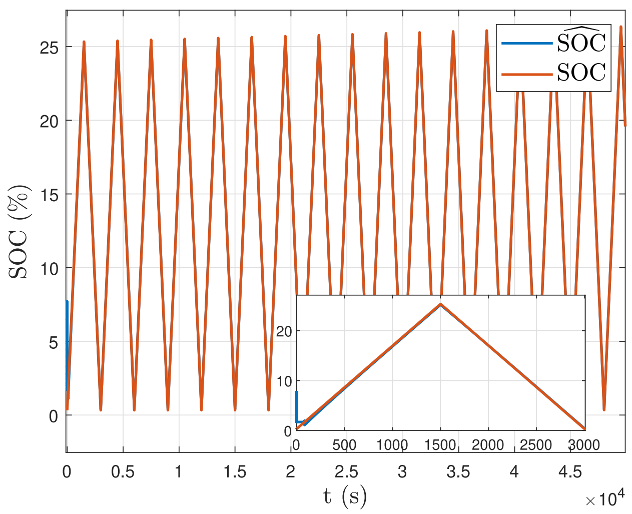

(a) SOC.

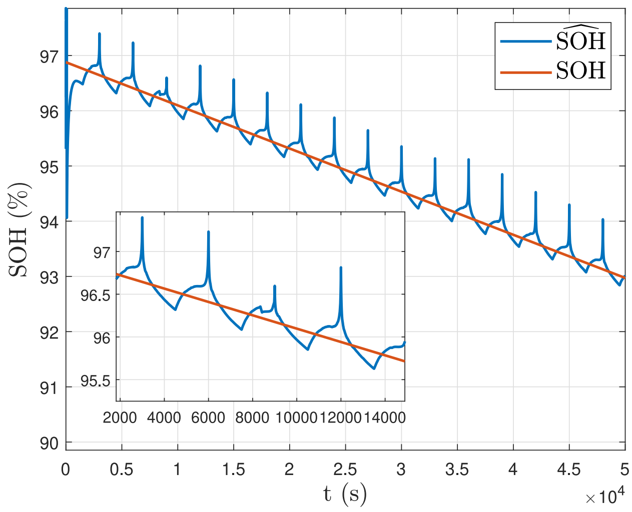

(b) SOH.

Fig. 6. Real (red) and estimated (blue) SOC and SOH dynamics when n_+ decreases along the time but is assumed constant in the reduced 2nd order-model. (For interpretation of the references to color in this figure legend, the reader is referred to the web version of this article.)

new system dynamics using an augmented third-order model. This new model can be defined as follows:

$$\dot{\boldsymbol{x}} = \begin{bmatrix} \dfrac{I}{v^{elec} \cdot F} \\ \delta \\ 0 \end{bmatrix} \tag{38}$$

$$y = h(\boldsymbol{x_2}, n, \varsigma, n_+)$$

being $\boldsymbol{x} = [x_2 \; n_+ \; \delta]^\top$ the new state vector composed by the vanadium species x_2, the number of vanadium moles in the positive side n_+, and a parameter δ that determines the slope of the SOH decline. Thus, the system becomes a third order-model.

Under the formulation of these new dynamics, it is possible to design a third-order SMO that accomplish with the same objectives described. Developing the observability analysis it is possible to obtain that the rank of the observability codistribution matrix Ω_s for the system formulated in (38) is 3. Therefore, the new system dynamics represented by (38) are still observable using the output y.

Following with the same procedure described for the observer design, it is possible to compute the estimation dynamics as:

$$\begin{aligned} \dot{\hat{z}}_0 &= \hat{z}_1 - \kappa_0 M^{1/3} |\hat{z}_0 - y|^{(2/3)} \cdot sign(\hat{z}_0 - y) \\ \dot{\hat{z}}_1 &= \hat{z}_2 - \kappa_1 M^{2/3} |\hat{z}_1 - \dot{\hat{z}}_0|^{(1/2)} \cdot sign(\hat{z}_1 - \dot{\hat{z}}_0) \\ \dot{\hat{z}}_2 &= -\kappa_2 M \cdot sign(\hat{z}_2 - \dot{\hat{z}}_1) \,, \end{aligned} \tag{39}$$

where appears a new parameter to be tuned with respect to the previous case which corresponds to κ_2. With respect to M, it must be chosen being greater than the upper bound of the third voltage derivative $\dddot{y}$, which can be found analytically performing the procedure described previously.

If the observer parameters are selected properly according to the theoretical specifications mentioned, it is possible to estimate both SOC and SOH with great accuracy as can be seen in Fig. 7. For this study, the original model is compared with the reduced one formulated by means of the system (38) when n_+ decreases along the time.

As can be observed in Fig. 7, the estimated SOC and SOH are compared with the real evolution using the original 4th order-model.

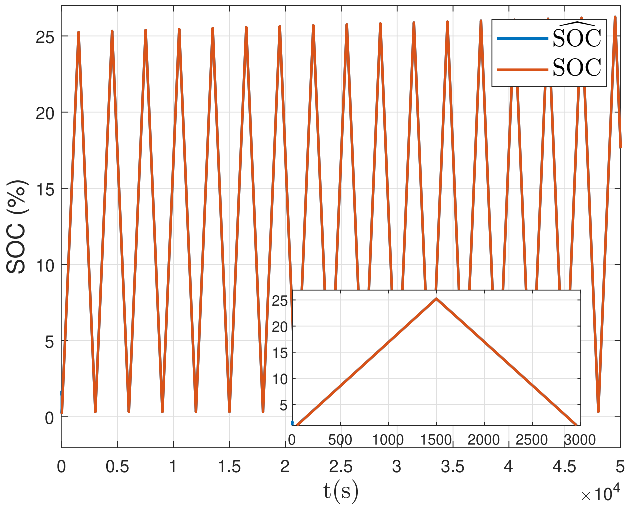

(a) SOC.

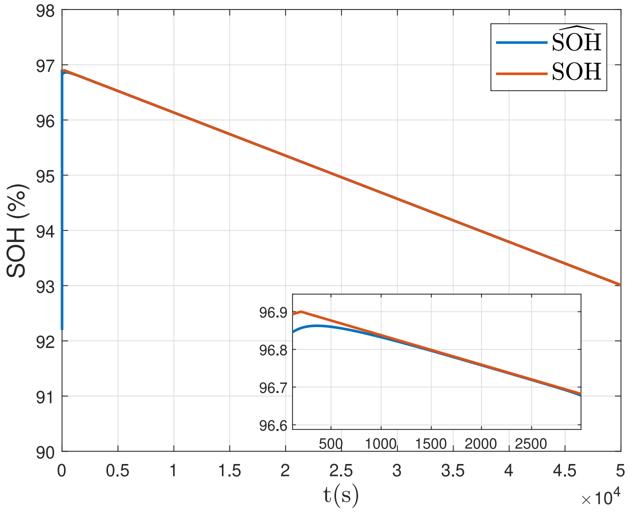

(b) SOH.

Fig. 7. Real (red) and estimated (blue) SOC and SOH dynamics when n_+ decreases and is considered a state in the reduced 3rd order-model. (For interpretation of the references to color in this figure legend, the reader is referred to the web version of this article.)

Fig. 7(a) shows the profiles of the real and estimated SOC during a charging and discharging process. With respect to the SOH, Fig. 7(b) shows the dynamics of this indicator, where it is also possible to check the same tendency regarding the error dynamics.

As can be seen, for this particular case, the SOH estimation converges to the real value with null steady state error. From these obtained results it is possible to conclude that the new dynamics obtained do not present error in the estimation of both SOC and SOH.

After validating the numerical analysis, the proposed observers can be implemented for a real VRFB system. However, before implementing these techniques, it is important to consider features such as computation time, convergence time, maximum acceptable error and the potential occurrence of chattering phenomenon.

Regarding the computation time, it depends on the number of operations that must be performed in each iteration. Therefore, for the purpose of this work, it can be associated with the computation of the observer states $\boldsymbol{z}$ presented in Eq. (29). Taking the worst-case scenario as an example, considering the 3rd-order model observer, it implies implementing a discretized version of Eq. (39). As observed, this process does not require complex computational costs, involving simple mathematical operations. Thus, these calculations can be performed in a matter of microseconds. Therefore, for real applications where the sampling periods can vary from milliseconds to seconds, the proposed observer can be used effectively.

With respect to the convergence time, it can be modified according to the observer gains, as mentioned and shown for the SOC estimation problem. With respect to the estimation of both SOC and SOH indicators, considering a complete charging and discharging cycle of 3000 s, the convergence time required to correctly estimate both indicators is less than 1000 s. Taking into account these results from the numerical analysis, it can be stated that the proposed observer can be used for real applications being possible to estimate both SOC and SOH indicators before a cycle ends. Additionally, it is important to emphasize that convergence time is required when initializing the observer from scratch, i.e. it will only affect during the first charging/discharging cycle.

In terms of the maximum allowable error, for high-scale energy systems such as the VRFB analyzed in this work, values lower than 1% are considered acceptable. As evident from the presented results, under conditions of noise disturbance and parameter uncertainty, it is possible to achieve lower errors results by adjusting the observer gains.

Finally, it is important to explain the possibility of phenomena such as chattering in real applications. This phenomenon is influenced by different factors such as the sampling period or the observer gain. With respect of the sampling period, it depends on the application. For our case of study, this sample period is only related with the measurement of both voltage and current measurements, being possible to work under sample periods between 0.1 to 1 s. The main problem when using low samples periods is a slower integration that implies more chattering in the estimated signals. In terms of the observer gain, higher values required to speed the convergence time also favor the appearance of chattering.

5. Experimental validation

To validate the results obtained from the numerical analysis, an experiment was conducted using a real VRFB prototype assembled at the Instituto de Carboquímica. The experimental setup comprises two reservoirs, each with a volume of 250 ml, and a stack consisting of 5 cells. Concerning the structure of the stack, each cell is composed of two PAN-based Sigracell® GFD4.6 felt electrodes thermally activated as described in [42], each with a surface area of 60 cm^2 and compressed 0.6 mm (from 4.6 to 4.0 mm). Each pair of electrodes is separated by a Fumasep FAP-450 membrane to separate the anode from the cathode reactions. Finally, the cells assembled in series are separated by flexible graphite bipolar plates manufactured by Mersen. Regarding the electrolyte composition, a solution of 1600 $\mathrm{mol/m}^3$ of vanadium in H_2SO_4 supplied by HydraRedox was used. Using two peristaltic pumps, the electrolytes were introduced at the bottom of the stack, distributed to the cells following a Z-type configuration and returned to the tanks from the top of the stack, ensuring that they reach the entire surface of the electrodes.

In order to prevent the oxidation of vanadium species V^{2+}, a nitrogen line is connected to the anolyte tank. Thus, the mass imbalance can be associated only to the ion crossover phenomenon through the membrane. Finally, with the purpose of validating the observer design it is necessary to compute the current and voltage along the time. Both measurements of current and voltage are monitored and saved using a Raspberry PLC with a sample time of 1 s. Fig. 8 shows the experimental setup with the aforementioned parts.

Before implementing the observer, as in any estimation problem, it is necessary to calibrate the model. For the case of a VRFB, typical parameters to be tuned are the standard potential E^{θ^*} and the ohmic resistances r_c and r_d. These parameters must be properly calibrated since they appear on the voltage computation as it was shown in

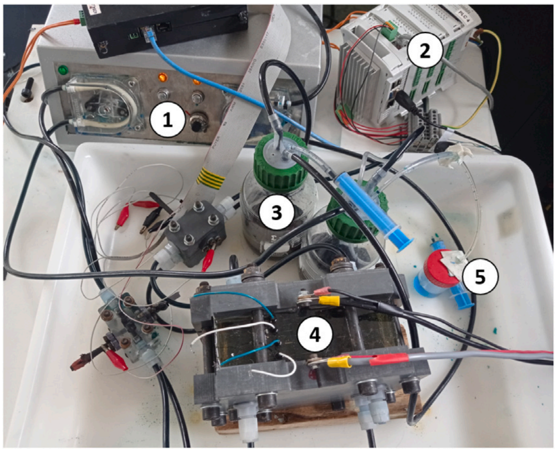

Fig. 8. VRFB prototype assembled in the Instituto de Carboquímica. 1: Peristaltic pumps; 2: Raspberry PLC; 3: Electrolyte reservoirs; 4: Stack; 5: Nitrogen line.

Eqs. (16) and (17). They have been calibrated using the PSO technique presented in different works [6,15,43]. The PSO technique is a computational method that iteratively improves possible solution candidates to optimize a given problem. Initially, these candidates form a swarm of particles, typically constrained by upper and lower values of the unknown parameters to be estimated. Each particle has a position and velocity that is updated in each iteration based on a cost function, allowing the identification of local and global minima in optimization problems. Therefore, once these bounds are defined, it is only necessary to establish the number of particles that will constitute the swarm. Increasing the number of particles ensures obtaining more accurate values but comes with a higher computational cost.

For our study, the propose vector of parameters to be estimated is $p = [E^{\theta^*}, r_c, r_d]$ and to solve this problem it has been defined a swarm of 400 particles with a lower bound vector $\underline{p} = [1, 0.01, 0.01]$, a upper bound vector $\overline{p} = [2, 1, 1]$ and using the mean square error (MSE) between the real and estimated voltages. Using the PSO solver of Matlab, the obtained results have been 1.35 V, 0.12 Ω and 0.14 Ω, for E^{θ^*}, r_c and r_d, respectively.

The experiments conducted to validate the observer involved different charging and discharging cycles at a constant current of 2 A, which represents a current density of 33.3 mA cm^{-2}. These operating conditions were selected for two main reasons. Firstly, VRFBs are commonly operated at constant voltage or constant current due to the limited battery voltage range [2], necessitating specific battery characterization for constant power operation [44]. Secondly, the use of constant current allows for a more precise definition of a charging and discharging cycle.

In relation to the SOC, the correlation with operating current density is only temporal. On the other hand, regarding SOH, it is possible that current densities may have varying influences on phenomena such as ion crossover or capacity decay. However, for the purposes of this study, there is no need to analyze other operating current densities. The primary reason is that, as explained earlier, the behavior of SOC and SOH remains nearly constant, yielding similar profiles albeit at different time intervals. Consequently, with higher current densities, the number of cycles increases compared to lower ones over the same period, potentially leading to a faster capacity decay in terms of SOH. The key point here is that these temporal differences do not interfere with the developed observer. As demonstrated in the numerical analysis, the convergence times for both SOC and SOH can be adjusted based on the observer gains. Consequently, using the aforementioned current allows for the definition of a complete cycle, involving a charging process until the voltage reaches 8 V, followed by a discharging process until the voltage reaches 4 V, as depicted in Fig. 9(a).

It must be highlighted that the proposed observer can operate under various operating conditions in terms of current and voltage, including the use of constant power profiles. This capability stems from its reliance solely on current and voltage measurements, without imposing limitations on the behavior of these signals. With respect to other experimental conditions, high flow rates of 350 ml min^{-1} where used to guarantee that the concentration inside the cell and tanks is equal.

Finally, in terms of temperature inside the stack, as could not be monitored is was assumed constant and equal to 298 K. Specific models have been developed in the literature to determine the temperature inside the cell or stack of a VRFB, considering the ambient temperature and the temperatures inside the electrolyte tanks, such as the one developed by Skyllas-Kazacos et al. [45]. However, in these works, it has been observed that the major contribution to temperature fluctuations is due to high current densities or extreme levels of SOC, as analyzed in the work of Trovo et al. [46]. Therefore, considering the low current density used for the experiments, it is possible to assume that the electrolyte temperature remains constant.

As can be noticed from Fig. 9(a) the period time of the cycles decreases over time due to the effect of the mass imbalance. Therefore, by means of this type of experiment it is possible to validate the proposed SOC and SOH observer at long term scenarios.

As the experimental data correspond to a long operational time, in order to estimate both SOC and SOH indicators, the model used is the ones presented in Eq. (39). For this case of study, the different values of the observer parameters used are: $\kappa_0 = 7$, $\kappa_1 = 20$, $\kappa_2 = 10$ and $M = 1 \cdot 10^{-3}$.

Fig. 9(b) shows the output estimation $\hat{y}$ compared to the real one measured y when the proposed observer is implemented. As can be noticed, the estimated output converges to the real one with practically null error in less than 100 s, which is a fast response and expected considering the numerical analysis made.

The observed SOC and SOH dynamics are shown in Fig. 9(c) where it can be seen how the SOH decreases while the SOC varies according to the charging process that takes place. For these simulations, the results have been plotted using the same sampling time period of 0.2 s. However, it has also been validated for a sampling time period of 1 s. As explained in the numerical section, the computation time is much smaller than these periods, making it possible to obtain a good estimation of both indicators before a cycle ends.

The proposed SOC and SOH observer can be validated computing the capacity loss along the cycles. In this work, the capacity loss during the charging process has been calculated by means of the Coulomb counting method.

Thus, the capacity can be computed in units of A s by the following equation:

$$C_k = \int_{t_k^0}^{t_k^f} I\, dt \tag{40}$$

where C_k is the capacity of a particular cycle k, t_k^0 is the initial time of the cycle k and t_k^f is the final time.

The computation of the capacity in each cycle has sense taking into account that all cycles are defined with the same operating conditions previously mentioned. Thus, it is possible to see how the capacity decay along the cycles. Fig. 10(a) shows the capacity evolution (red dots) with respect to the cycles. To have more knowledge about the capacity decay a linear function has been used to interpolate the data, being possible to see an approximately drop of 164 A s for cycle.

With respect to the initial capacity of the system, it is possible to compute the system capacity as:

$$C_0 = \frac{F \cdot c_t \cdot v^{elec}}{N} \tag{41}$$

where v^{elec} is the electrolyte volume which is 250 ml, N is 5 according to the number of cells of the stack and c_t is the total vanadium

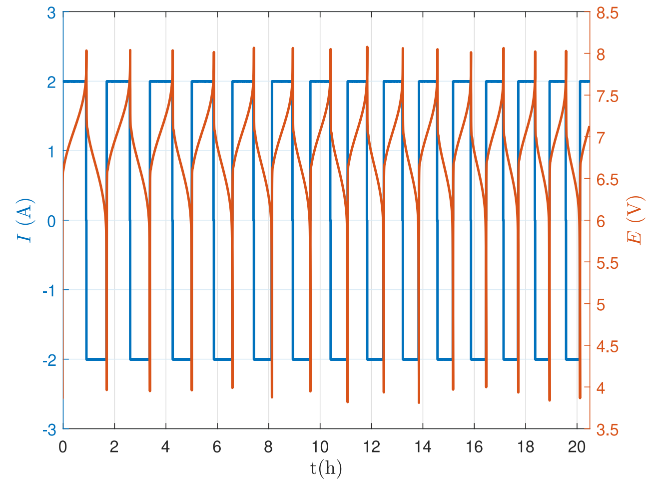

(a) Current and voltage measurements.

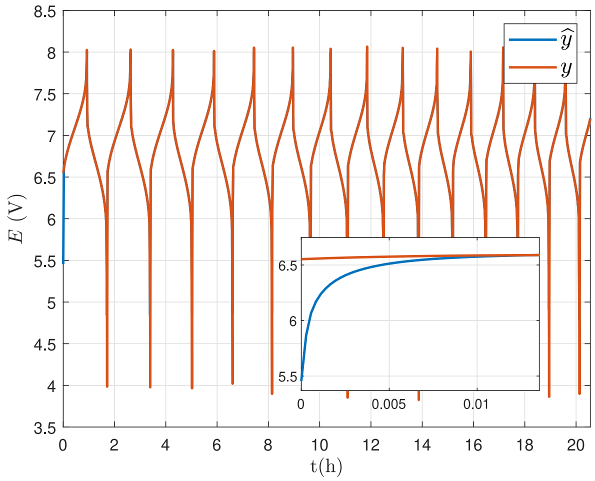

(b) Output voltage estimation.

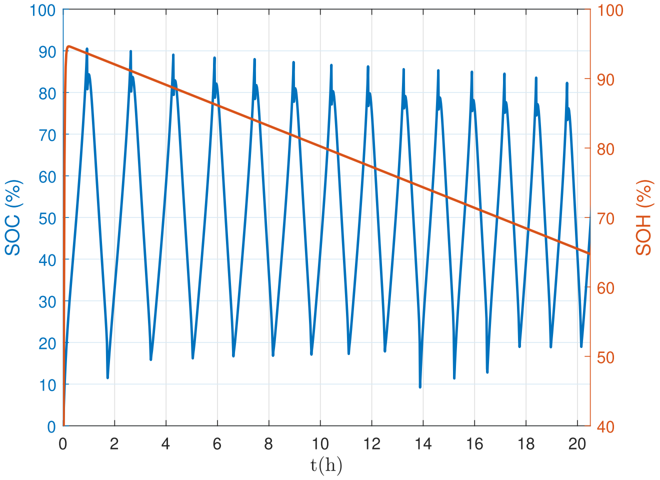

(c) SOC and SOH estimation.

Fig. 9. Experiment developed to estimate the SOC and SOH with the proposed observer during 14 cycles at constant current density of 33.3 mA/cm^2. (a) Current (blue) and voltage (red) measurements. (b) Real (red) and estimated (blue) output voltage. (c) SOC (blue) and SOH (red) estimations. (For interpretation of the references to color in this figure legend, the reader is referred to the web version of this article.)

Table 1
Observer design parameters.

Notation	Meaning
κ	Observer coefficient
M	Observer coefficient
Φ	Jacobian matrix
f	System dynamics function
h	Output system function
L	Lie derivative
u	System inputs
x	System state vector
$\hat{\mathrm{x}}$	State estimation
$\dot{\mathrm{x}}$	State derivative
y	System output measurement

Table 2
VRFB model parameters.

Notation	Meaning	Units
E	VRFB voltage	V
E^{θ}	Standard electrode potential	V
F	Faraday's constant	A s/mol
I	VRFB current	A
N	Number of cells	–
n	Moles of vanadium species	–
n_-	Anolyte moles of species	–
n_+	Catholyte moles of species	–
R	Constant of gases	J/mol K
r_c	Charging resistance	Ω
r_d	Discharging resistance	Ω
SOC	State of Charge	- or %
SOH	State of Health	- or %
T	Temperature	K
v^{elec}	Electrolyte volume	m^3
v^c	Cell volume	m^3
v^t	Tank volume	m^3
x	Species concentration	mol/m^3

concentration which is 1600 mol/m^3. Then, the theoretical initial capacity of the VRFB is 7718 A s. This value is far from the initial experimental value (6685 A s). There are different reasons that explain this difference.

On the one hand, it is possible that during the first cycle there is a loss of capacity. However, as has been observed in Fig. 10(a), the capacity is around 164 A s. On the other hand, the theoretical initial capacity computed by Eq. (41) considers that all vanadium species react according to the total vanadium concentration c_t. Nevertheless, to operate the system in optimal and safe conditions the SOC does not usually reach 100% where high overpotentials appear and side reactions can take place. This SOC limitation can be found looking at Fig. 9(a) where the maximum voltage reaches 8 V that corresponds to 1.6 V per cell. According to the literature, this voltage value is associated to a 90% SOC. Therefore, the theoretical initial capacity must be computed considering this SOC limitation obtaining a value of 6946.92 A s which is closer to the experimental one.

Computing the capacity in units of SOH, it is possible to compare the experimental SOH obtained from Fig. 10(a) with the estimated one by the implemented observer that appears in Fig. 9(c). Both profiles are shown in Fig. 10(b) where it is possible to see how the estimated SOH matches with the one obtained from the Coulomb counting method. As can be noticed, at initial state when the SOH is totally unknown there exist an important error between the real and estimated value. However, after 500 s the SOH stabilizes near the real value. It is important to remark that the use of the Coulomb counting method to validate the SOH estimation has its limitations when a battery is used over an extended period without undergoing full charge or discharge cycles. As the battery operates over time, errors accumulate, posing difficulties in accurately estimating the SOH. It is plausible that running the cell for an extended duration may lead to more pronounced deviations as the ones shown at the end of the experiment.

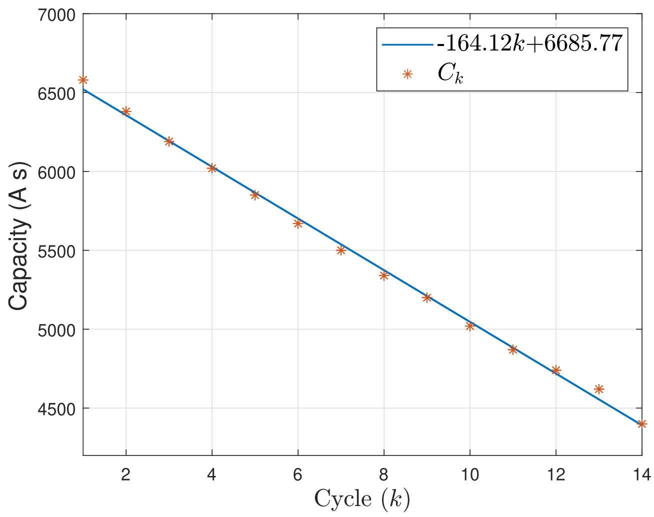

(a) Capacity decay.

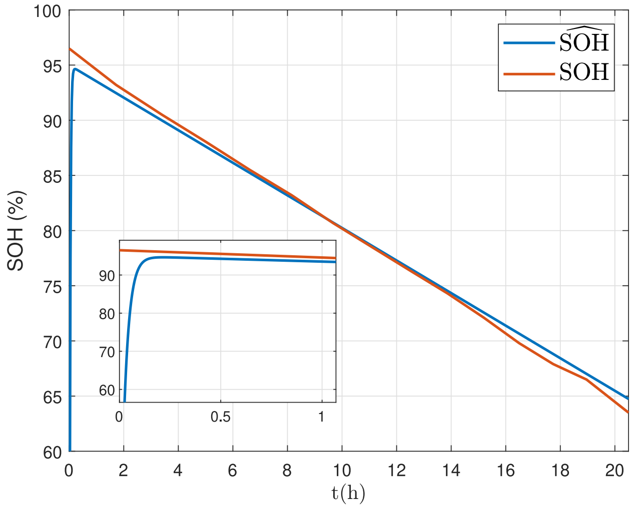

(b) SOH comparison.

Fig. 10. Analysis of the SOH estimation. (a) Experimental capacity decay at each cycle (red) and the interpolated linear function of all this points (blue). (b) Experimental SOH obtained from Coulomb counting method (red) and the estimated one (blue) using the proposed observer with the system dynamics (38). (For interpretation of the references to color in this figure legend, the reader is referred to the web version of this article.)

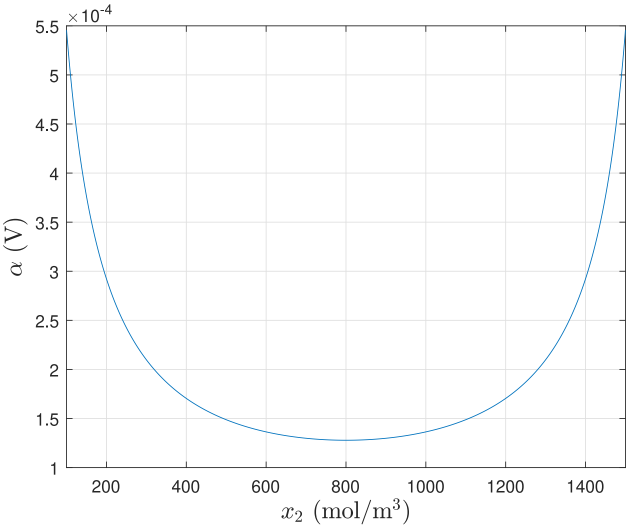

(a) Evolution of α.

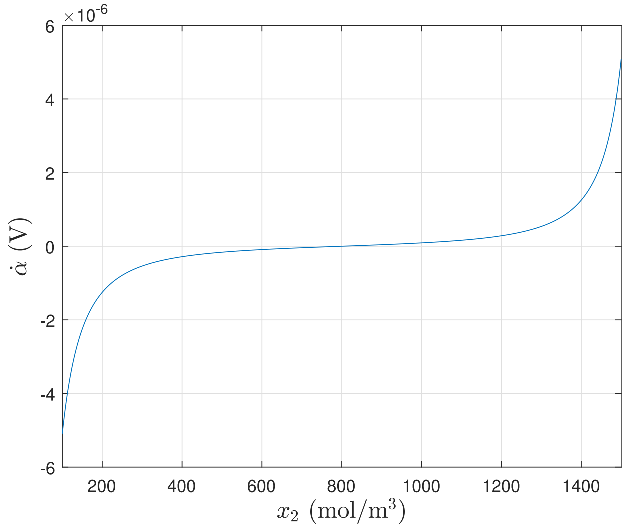

(b) Evolution of $\dot{\alpha}$.

Fig. 11. Evolution of α and its derivative considering that the operating region varies between 10 to 90% of SOC. (a) Evolution of α. (b) Evolution of $\dot{\alpha}$.

6. Conclusions

In this research, an online state of charge (SOC) and state of health (SOH) estimation technique is proposed based on a recognized electrochemical model proposed by Skyllas-Kazacos et al. [47]. By means of the conservation laws, a reduced order-model can be used for both SOC and SOH monitoring using the current as input and the battery voltage as output measure. The reduced-order model takes into account various phenomena, including redox reactions, the impact of flow rates, and mass imbalance. While the proposed model has limitations in terms of addressing battery degradation or electrochemical inefficiencies, its operation in a closed-loop observer enables it to compensate for these undesired phenomena. The proposed observer consists on a high-gain sliding mode observer (HGSMO) that presents a null steady-state error and can be tuned in order to avoid some parameter uncertainty or measurement noise. One of the strengths of the proposed observer is that it only requires the measurement of the battery voltage, which is a variable that can be measured with great accuracy and with practically null noise, as has been observed in the experimental part.

The experimental validation has shown reasonably good results when the estimated SOH has been compared to the real one, obtaining a relative error less than 2%. These results demonstrate a high level of accuracy in addressing the SOC and SOH estimation problem compared to other works that rely on equivalent circuit models (ECMs) and solely utilize the open-circuit voltage (OCV) measurement. However, the importance of knowing the total concentration of vanadium species must be remarked in order to properly apply the conservation principles. For future contributions it could be interesting to analyze different aspects. On one hand, in light of the challenges associated with the Coulomb counting approach to validate the SOH estimation, it could be necessary to conduct complete charge or discharge processes to more accurately quantify the real capacity when determining the SOH. Furthermore, it is conceivable that certain model parameters may undergo changes with repeated cycles. A pragmatic approach to recalibrating the observer could involve performing a single cycle to re-estimate the model parameters and subsequently implementing the observer again using this newly parameterized model.

CRediT authorship contribution statement

Alejandro Clemente: Methodology, Software, Writing – original draft. **Manuel Montiel:** Conceptualization, Data curation, Formal analysis, Investigation, Resources, Writing – original draft. **Félix Barreras:** Conceptualization, Funding acquisition, Investigation, Project administration, Writing – review & editing. **Antonio Lozano:** Conceptualization, Funding acquisition, Investigation, Methodology, Writing – review & editing. **Bryan Escachx:** Investigation, Software, Writing – original draft. **Ramon Costa-Castelló:** Conceptualization, Funding acquisition, Investigation, Resources, Writing – review & editing.

Declaration of competing interest

The authors declare that they have no known competing financial interests or personal relationships that could have appeared to influence the work reported in this paper.

Data availability

Data will be made available on request.

Acknowledgments

This research has been developed within the CSIC Interdisciplinary Thematic Platform (PTI+) Transición Energética Sostenible+ (PTI-TRANSENER+) as part of the CSIC program for the Spanish Recovery, Transformation and Resilience Plan funded by the Recovery and Resilience Facility of the European Union, established by the Regulation (EU) 2020/2094, the Spanish Ministry of Science and Innovation under projects MAFALDA (PID2021-126001OB-C31 and C32 funded by MCIN/AEI/ 10.13039/501100011033/ERDF, EU) and MASHED (TED2021-129927B-I00), the European Union's H2020 research and innovation programme under grant agreement number 963652 Project HYBRIS and by the Spanish Ministry of Universities funded by the European Union - NextGenerationEU (2022UPC-MSC-93823).

Appendix

In order to compute numerically the value of the output derivative $\dot{y}$, and its respective derivatives, the following procedure can be developed.

First of all, starting from the original system (22), it is possible to rewrite the problem as:

$$\begin{aligned} \dot{x}_2 &= \lambda \cdot I \\ y &= h(x_2, I)\ , \end{aligned} \tag{42}$$

where λ is a constant that according to (22) is defined as $\lambda = 1/F \cdot v^{elec}$.

Then, it is possible to compute the output derivative, $\dot{y}$, as:

$$\dot{y} = \frac{\partial h}{\partial x_2} \cdot \dot{x}_2 + \frac{\partial h}{\partial I} \cdot \dot{I}, \tag{43}$$

which can be rewritten as:

$$\dot{y} = \alpha(x_2) \cdot \lambda \cdot I + r \cdot \dot{I}\ , \tag{44}$$

where α denotes the partial derivative of h with respect to x_2 and r is the ohmic resistor according to (16).

The value of α can be computed numerically, developing the partial derivative of h with respect to x_2 and considering the possible values of x_2. Fig. 11(a) shows the numerical values of α with respect to x_2, considering the parameters defined in the numerical section and that the SOC can only vary between 10 to 90%.

Thus, it is possible to obtain the upper value of $\dot{y}$ with respect to the input current I as:

$$\|\dot{y}\| \leq 5.5 \cdot 10^{-4} \cdot \lambda \cdot \|I\| + r \cdot \|\dot{I}\|\ . \tag{45}$$

As can be noticed, by means of this procedure it is only necessary to take into account the profile of the input current I, and its derivatives.

The second derivative $\ddot{y}$ can be computed according to (44) as:

$$\begin{aligned} \ddot{y} &= \frac{\partial \alpha}{\partial x_2} \cdot \dot{x}_2 \cdot \lambda \cdot I + \alpha(x_2) \cdot \lambda \cdot \dot{I} + r \cdot \ddot{I} && (46) \\ &= \frac{\partial \alpha}{\partial x_2} \cdot \lambda^2 \cdot I^2 + \alpha(x_2) \cdot \lambda \cdot \dot{I} + r \cdot \ddot{I}\ , && (47) \end{aligned}$$

being possible to compute the upper value of $\ddot{y}$ considering the upper value of the derivative of α with respect x_2 (Fig. 11(b)) as:

$$\|\ddot{y}\| \leq 6 \cdot 10^{-6} \cdot \lambda^2 \cdot I^2 + 5.5 \cdot 10^{-4} \cdot \lambda \cdot \|\dot{I}\| + r \cdot \|\ddot{I}\|\ . \tag{48}$$

Following this procedure, higher derivatives can be computed and the upper value M can be adjusted with respect to a particular known input current I.

Nomenclature

See Tables 1 and 2.

References

[1] A. Clemente, R. Costa-Castelló, Redox flow batteries: A literature review oriented to automatic control, Energies 13 (2020) 4514, http://dx.doi.org/10.3390/en13174514.

[2] T. Puleston, A. Clemente, R. Costa-Castelló, M. Serra, Modelling and estimation of vanadium redox flow batteries: A review, Batteries 8 (9) (2022) http://dx.doi.org/10.3390/batteries8090121.

[3] M. Skyllas-Kazacos, M. Kazacos, State of charge monitoring methods for vanadium redox flow battery control, J. Power Sources 196 (20) (2011) 8822–8827, http://dx.doi.org/10.1016/j.jpowsour.2011.06.080.

[4] K.-H. Shin, C.-S. Jin, J.-Y. So, S.-K. Park, D.-H. Kim, S.-H. Yeon, Real-time monitoring of the state of charge (SOC) in vanadium redox-flow batteries using UV–Vis spectroscopy in operando mode, J. Energy Storage 27 (2020) 101066, http://dx.doi.org/10.1016/j.est.2019.101066.

[5] R. Weber, C. Schubert, B. Poisl, K.-H. Pettinger, Analyzing experimental design and input data variation of a vanadium redox flow battery model, Batteries 9 (2) (2023) http://dx.doi.org/10.3390/batteries9020122.

[6] A. Clemente, M. Montiel, F. Barreras, A. Lozano, R. Costa-Castelló, Vanadium redox flow battery state of charge estimation using a concentration model and a sliding mode observer, IEEE Access 9 (2021) 72368–72376, http://dx.doi.org/10.1109/ACCESS.2021.3079382.

[7] B. Xiong, J. Zhao, Z. Wei, M. Skyllas-Kazacos, Extended Kalman filter method for state of charge estimation of vanadium redox flow battery using thermal-dependent electrical model, J. Power Sources 262 (2014) 50–61, http://dx.doi.org/10.1016/j.jpowsour.2014.03.110.

[8] B. Xiong, J. Zhao, Y. Su, Z. Wei, M. Skyllas-Kazacos, State of charge estimation of vanadium redox flow battery based on sliding mode observer and dynamic model including capacity fading factor, IEEE Trans. Sustain. Energy 8 (4) (2017) 1658–1667, http://dx.doi.org/10.1109/TSTE.2017.2699288.

[9] S. Dong, J. Feng, Y. Zhang, S. Tong, J. Tang, B. Xiong, State of charge estimation of vanadium redox flow battery based on online equivalent circuit model, in: 2021 31st Australasian Universities Power Engineering Conference, AUPEC, 2021, pp. 1–6, http://dx.doi.org/10.1109/AUPEC52110.2021.9597837.

[10] Z. Wei, F. Leng, Z. He, W. Zhang, K. Li, Online state of charge and state of health estimation for a lithium-ion battery based on a data–model fusion method, Energies 11 (7) (2018) http://dx.doi.org/10.3390/en11071810.

[11] B. Khaki, P. Das, Fast and simplified algorithms for SoC and SoH estimation of vanadium redox flow batteries, in: 2021 IEEE Green Technologies Conference, GreenTech, 2021, pp. 494–501, http://dx.doi.org/10.1109/GreenTech48523.2021.00083.

[12] Z. Wei, K.J. Tseng, N. Wai, T.M. Lim, M. Skyllas-Kazacos, Adaptive estimation of state of charge and capacity with online identified battery model for vanadium redox flow battery, J. Power Sources 332 (2016) 389–398, http://dx.doi.org/10.1016/j.jpowsour.2016.09.123.

[13] V. Vlasov, M. Pugach, D. Kopylova, A. Novikov, N. Gvozdik, A. Mkrtchyan, A. Davletkhanov, Y. Gladush, F. Ibanez, D. Gorin, K. Stevenson, In situ state of health vanadium redox flow battery deterministic method in cycling operation for battery capacity monitoring, J. Power Sources 584 (2023) 233600, http://dx.doi.org/10.1016/j.jpowsour.2023.233600.

[14] T. Puleston, A. Cecilia, R. Costa-Castelló, M. Serra, Vanadium redox flow batteries real-time state of charge and state of health estimation under electrolyte imbalance condition, J. Energy Storage 68 (2023) 107666, http://dx.doi.org/10.1016/j.est.2023.107666.

[15] A. Clemente, M. Montiel, F. Barreras, A. Lozano, R. Costa-Castelló, Experimental validation of a vanadium redox flow battery model for state of charge and state of health estimation, Electrochim. Acta 449 (2023) 142117, http://dx.doi.org/10.1016/j.electacta.2023.142117.

[16] R. Badrinarayanan, J. Zhao, K. Tseng, M. Skyllas-Kazacos, Extended dynamic model for ion diffusion in all-vanadium redox flow battery including the effects of temperature and bulk electrolyte transfer, J. Power Sources 270 (2014) 576–586, http://dx.doi.org/10.1016/j.jpowsour.2014.07.128.

[17] N.M. Delgado, R. Monteiro, J. Cruz, A. Bentien, A. Mendes, Shunt currents in vanadium redox flow batteries – a parametric and optimization study, Electrochim. Acta 403 (2022) 139667, http://dx.doi.org/10.1016/j.electacta.2021.139667.

[18] K.B. Oldham, C.G. Zoski, Chapter 2 mass transport to electrodes, in: C. Bamford, R. Compton (Eds.), Electrode Kinetics: Principles and Methodology, in: Comprehensive Chemical Kinetics, vol. 26, Elsevier, 1986, pp. 79–143, http://dx.doi.org/10.1016/S0069-8040(08)70026-8.

[19] L. Hao, Y. Wang, Y. He, Modeling of ion crossover in an all-vanadium redox flow battery with the interfacial effect at membrane/electrode interfaces, J. Electrochem. Soc. 166 (2019) A1310–A1322, http://dx.doi.org/10.1149/2.1061906jes.

[20] Y.-S. Chou, S. Yen, A. Arpornwichanop, B. Singh, Y.-S. Chen, Mathematical model to study vanadium ion crossover in an all-vanadium redox flow battery, ACS Sustain. Chem. Eng. 9 (2021) http://dx.doi.org/10.1021/acssuschemeng.1c00233.

[21] K. Oh, M. Moazzam, G. Gwak, H. Ju, Water crossover phenomena in all-vanadium redox flow batteries, Electrochim. Acta 297 (2019) 101–111, http://dx.doi.org/10.1016/j.electacta.2018.11.151.

[22] C.-N. Sun, F. Delnick, L. Baggetto, G. Veith, T. Zawodzinski, Hydrogen evolution at the negative electrode of the all-vanadium redox flow batteries, J. Power Sources 248 (2013) 560, http://dx.doi.org/10.1016/j.jpowsour.2013.09.125.

[23] K. Knehr, E. Kumbur, Open circuit voltage of vanadium redox flow batteries: Discrepancy between models and experiments, Electrochem. Commun. 13 (4) (2011) 342–345, http://dx.doi.org/10.1016/j.elecom.2011.01.020.

[24] J. Langner, J. Melke, H. Ehrenberg, C. Roth, Determination of overpotentials in all vanadium redox flow batteries, ECS Trans. 58 (37) (2014) 1, http://dx.doi.org/10.1149/05837.0001ecst.

[25] A. Pezeshki, J. Clement, G. Veith, T. Zawodzinski, M. Mench, High performance electrodes in vanadium redox flow batteries through oxygen-enriched thermal activation, J. Power Sources 294 (2015) http://dx.doi.org/10.1016/j.jpowsour.2015.05.118.

[26] N.M. Delgado, R. Monteiro, M. Abdollahzadeh, P. Ribeirinha, A. Bentien, A. Mendes, 2D-dynamic phenomenological modelling of vanadium redox flow batteries – analysis of the mass transport related overpotentials, J. Power Sources 480 (2020) 229142, http://dx.doi.org/10.1016/j.jpowsour.2020.229142.

[27] D. Noren, M. Hoffman, Clarifying the Butler–Volmer equation and related approximations for calculating activation losses in solid oxide fuel cell models, J. Power Sources 152 (2005) 175–181, http://dx.doi.org/10.1016/j.jpowsour.2005.03.174.

[28] C. Alegre, A. Lozano, Ángel Pérez Manso, L. Álvarez-Manuel, F.F. Marzo, F. Barreras, Single cell induced starvation in a high temperature proton exchange membrane fuel cell stack, Appl. Energy 250 (2019) 1176–1189, http://dx.doi.org/10.1016/j.apenergy.2019.05.061.

[29] A. Levant, Higher-order sliding modes, differentiation and output-feedback control, Int. J. Control - Int. J. Control 76 (2003) 924–941, http://dx.doi.org/10.1080/0020717031000099029.

[30] S. Spurgeon, Sliding mode observers: A survey, Int. J. Syst. Sci. 39 (2008) 751–764, http://dx.doi.org/10.1080/00207720701847638.

[31] J. Du, Z. Liu, Y. Wang, C. Wen, An adaptive sliding mode observer for lithium-ion battery state of charge and state of health estimation in electric vehicles, Control Eng. Pract. 54 (2016) 81–90, http://dx.doi.org/10.1016/j.conengprac.2016.05.014.

[32] B. Xiong, H. Zhang, X. Deng, J. Tang, State of charge estimation based on sliding mode observer for vanadium redox flow battery, in: 2017 IEEE Power & Energy Society General Meeting, 2017, pp. 1–5, http://dx.doi.org/10.1109/PESGM.2017.8274042.

[33] A. Cecilia, S. Sahoo, T. Dragičević, R. Costa-Castelló, F. Blaabjerg, Detection and mitigation of false data in cooperative DC microgrids with unknown constant power loads, IEEE Trans. Power Electron. 36 (8) (2021) 9565–9577, http://dx.doi.org/10.1109/TPEL.2021.3053845.

[34] J. Davila, L. Fridman, A. Pisano, E. Usai, Finite-time state observation for non-linear uncertain systems via higher-order sliding modes, Internat. J. Control 82 (8) (2009) 1564–1574, http://dx.doi.org/10.1080/00207170802590531.

[35] E. Cruz-Zavala, J. Moreno, Levant's arbitrary order exact differentiator: A Lyapunov approach, IEEE Trans. Automat. Control PP (2018) 1, http://dx.doi.org/10.1109/TAC.2018.2874721.

[36] Y. Shtessel, C. Edwards, L. Fridman, A. Levant, Sliding Mode Control and Observation, Series: Control Engineering, Birkhauser:Basel, 2016, http://dx.doi.org/10.1007/978-0-8176-4893-0.

[37] N. Xuan Mung, N. Nguyen, B. Pham, N.-N. Dao, H. Nguyen, T. Ngoc, M. The Vu, S. Hong, Novel gain-tuning for sliding mode control of second-order mechanical systems: theory and experiments, Sci. Rep. 13 (2023) http://dx.doi.org/10.1038/s41598-023-37562-7.

[38] G. Besançon, Nonlinear Observers and Applications, vol. 363, Springer, 2007.

[39] J.-Y. Chen, C.-L. Hsieh, N.-Y. Hsu, Y.-S. Chou, Y.-S. Chen, Determining the limiting current density of vanadium redox flow batteries, Energies 7 (9) (2014) 5863–5873, http://dx.doi.org/10.3390/en7095863.

[40] E. García-Quismondo, I. Almonacid, M. Martínez, V. Miroslavov, E. Serrano, J. Palma, J. Salmerón, Operational experience of 5 kW/5 kWh all-vanadium flow batteries in photovoltaic grid applications, Batteries 5 (2019) 52, http://dx.doi.org/10.3390/batteries5030052.

[41] J.X. Shuang Zhang, R. Zhang, C.W. Zonghao Liu, R. Liu, M. Rong, State-of-health characteristics of all-vanadium redox flow batteries, Energy Storage Sci. Technol. 11 (12) (2022) 4022–4029, http://dx.doi.org/10.19799/j.cnki.2095-4239.2022.0409.

[42] J.E. Barranco, A. Cherkaoui, M. Montiel, A. González-Espinosa, A. Lozano, F. Barreras, Analysis of the electrochemical performance of carbon felt electrodes for vanadium redox flow batteries, Electrochim. Acta 470 (2023) 143281, http://dx.doi.org/10.1016/j.electacta.2023.143281.

[43] A. Clemente, A. Cecilia, R. Costa-Castelló, Online state of charge estimation for a vanadium redox flow battery with unequal flow rates, J. Energy Storage 60 (2023) 106503, http://dx.doi.org/10.1016/j.est.2022.106503.

[44] P.K. Vudisi, S. Jayanti, R. Chetty, Model for rating a vanadium redox flow battery stack through constant power charge:Discharge characterization, Batteries 8 (8) (2022) https://www.mdpi.com/2313-0105/8/8/85.

[45] A. Tang, S. Ting, J. Bao, M. Skyllas-Kazacos, Thermal modelling and simulation of the all-vanadium redox flow battery, J. Power Sources 203 (2012) 165–176, http://dx.doi.org/10.1016/j.jpowsour.2011.11.079.

[46] A. Trovò, A. Saccardo, M. Giomo, M. Guarnieri, Thermal modeling of industrial-scale vanadium redox flow batteries in high-current operations, J. Power Sources 424 (2019) 204–214, http://dx.doi.org/10.1016/j.jpowsour.2019.03.080.

[47] Y. Yan, Y. Li, M. Skyllas-Kazacos, J. Bao, Modelling and simulation of thermal behaviour of vanadium redox flow battery, J. Power Sources 322 (2016) 116–128, http://dx.doi.org/10.1016/j.jpowsour.2016.05.011.